Joint Coverage and Detection Performance Metrics for Integrated Sensing and Communication in Automotive Scenarios

François De Saint Moulin*, Charles Wiame†, Luc Vandendorpe‡, Claude Oestges§
ICTEAM, UCLouvain - Louvain-la-Neuve, Belgium
*francois.desaintmoulin@uclouvain.be, †charles.wiame@uclouvain.be,
‡luc.vandendorpe@uclouvain.be, §claude.oestges@uclouvain.be

***Abstract*—In this paper, novel performance metrics are introduced to analyse full-duplex integrated sensing and communication systems. Unlike previous studies, these metrics simultaneously capture the joint statistics achieved by both sensing and communication functions. First, using stochastic geometry, an automotive scenario involving joint radar-communication systems is introduced, in which a vehicle simultaneously detects the next vehicle ahead while receiving a communication signal from a road side unit. Next, the performance metrics are validated using Monte-Carlo simulations and trade-offs between both functions are highlighted. Then, the optimisation of the network node power and density is investigated to maximise the joint performance. Finally, the proposed framework is extended to include mutual interference cancellation capabilities between both functions. The cases of perfect and imperfect cancellation are both analysed. Other extensions and generalisations are also discussed.**

***Index Terms*—DFRC, ISAC, radar, communication, interference cancellation, automotive scenario, stochastic geometry**

I. Introduction

In recent years, with the spectrum scarcity and the convergence of the carrier frequency ranges used by radar and communication systems, the possibility to operate both functions using the same resources has received an increased attention. Joint radar-communication systems enable to perform both functions simultaneously with a single hardware platform [1], [2]. Two approaches have been adopted: coexistence and co-design. In the former, different waveforms are used for each function, and mutual interference between both functions must be mitigated. In the latter, a single waveform is transmitted, and trade-offs are made in the waveform design between both functions. Such systems are commonly named Dual Function Radar-Communication (DFRC) systems. In the particular case of vehicular networks, Vehicle-to-everything (V2X) networks are a key element to make vehicles smarter, and potentially autonomous. A lot of research is performed in these networks since they have the potential to improve the safety and the driving experience of road users. However, both high-accuracy localisation and high-throughput communication are required. This motivates the use of DFRC systems to alleviate spectrum congestion issues, reduce the hardware required on V2X network nodes, while potentially enabling to improve the performance achieved at both functions, possibly with cooperation [3]. However, the performance of both functions in such networks must be evaluated in order to design such systems.

François De Saint Moulin is a Research Fellow of the Fonds de la Recherche Scientifique - FNRS.

A. Related works

For communication applications, several performance metrics which are evaluated include the coverage probability, the spectral efficiency, the energy efficiency and the total received power. The joint evaluation of multiple metrics has also been considered, i.e. the achieved rate in uplink and downlink [4], or the simultaneous wireless information and power transfer [5]. For radar applications, stochastic geometry has been used to evaluate radar metrics (i.e. the false alarm, the detection and the success probability) and study the impact of multiple parameters in different scenarios. For instance, [6] analyses the Cumulative Distribution Function (CDF) of the interference with a population of pulsed-radar devices, [7]–[9] consider the radar performance in a cluttered environment, and [10] evaluates the detection probability when multiple obstacles are distributed around the radar systems.

Considering joint radar and communication applications, some works have been published regarding either coexisting radar and communication or co-designed systems. In the first case with coexisting systems, [11], [12] evaluate the radar range and the communication success probability of a joint radar-communication network with Time Division Multiple Access (TDMA). The interference from a rotating radar sharing the same spectrum as a cellular system is considered in [13], while [14] analyses the interference of a massive Multiple Input Multiple Output (MIMO) cellular network on a radar system. Finally, the development of cooperative multi-point detection is presented in [15], [16]. In the second case with co-designed systems, [17] evaluates the cooperative detection volume of a joint radar-communication system where targets are detected with the main beam and different stations cooperate by communicating through the secondary beams. The increase of communication throughput with joint radar-communication systems is evaluated in [18], and an analytical framework to optimise the system parameters is proposed.

In this work, stochastic geometry has been used as the main framework to analyse the considered network at a large scale level. This branch of spatial statistics abstracts network nodes positions as random point processes. Leveraging on this mathematical tool, closed-form expressions for performance metrics can be derived and averaged over all potential realisations of these point processes [19]–[23]. Using this framework, many automotive scenarios have been studied. First, for radar applications only, [24] compares the performance obtained with different random Radar Cross Section (RCS) models. To model the position of the vehicles, instead of using Poisson Point Processes (PPP), [25] proposes to use a one-dimensional lattice, and [26] uses Matérn hard-core processes in two dimensions. In [27], an arbitrary number of lanes in both directions is considered, and the reflected interference from vehicles on neighbouring lanes is taken into account. In [28], a multiple lane scenario is also considered, with front- and side-mounted radars with directional antenna patterns. To obtain a fine-grained analysis, [29], [30] evaluate the meta distribution of the Signal to Interference plus Noise Ratio (SINR), which enables to analyse the reliability of the detection at each individual vehicle. Regarding joint radar and communication applications, the cooperative detection range is evaluated in [31] and [32], respectively with spectrum allocation between both functions or with a joint radar-communication system. This range is defined as the total range in which targets are detected by multiple vehicles communicating with each other.

To our best knowledge, the joint statistics of both radar and communication functions in a single DFRC system have not been investigated so far. Such an analysis is required since (i) both functions mutually interfere, requiring a joint evaluation of the performance achieved by both functions as they are highly correlated, (ii) in addition to recovering the univariate metrics, conditional metrics can be defined from joint metrics, enabling to study the performance of one function given a requirement on the other function, and (iii) joint metrics enable to provide a single objective function to optimise DFRC systems parameters which takes into account both functions simultaneously without introducing any additional constraint, or to integrate the constraints into the objective function with the conditional metrics.

B. Contributions

Based on the aforementioned works, the contributions of this paper are summarised as follows:

- We introduce a new full-duplex scenario in which a typical node is receiving and processing simultaneously radar and communication signals, as shown in Figure 1. For the radar (resp. communication) function, the communication signal (resp. radar echo) is considered as an interference. However, this interference can be mitigated if both functions cooperate with each other. This configuration is applied in a two-lane road automotive scenario involving Road Side Units (RSU) and vehicles equipped with joint radar-communication systems, as illustrated in Figure 2. In this work, by means of the stochastic geometry framework, we evaluate the performance achieved for a typical vehicle receiving a communication signal from the RSUs while simultaneously detecting the next vehicle in the same lane.
- For this new scenario, multiple single-objective metrics are computed and validated with Monte-Carlo simulations, namely (i) the *communication coverage probability*, i.e. the probability for the communication SINR to reach a given requirement, (ii) the *radar false alarm probability*, i.e. the probability for the radar receiver to falsely detect a target which doesn't exist, (iii) the *radar detection probability*, i.e. the probability for the radar receiver to detect a real target, and (iv) the *radar success probability*, i.e. the probability for the radar to reach a given SINR requirement. These metrics enable to separately evaluate the performance of each function.
- We propose two new joint metrics, namely (i) the *Joint Radar Detection and Communication Coverage Probability* (JRDCCP), i.e. the probability to detect a target with a given false alarm probability at the radar function, while achieving a sufficient SINR at the communication function, and (ii) the *Joint Radar Success and Communication Coverage Probability* (JRSCCP), i.e. the probability to achieve simultaneously sufficient SINRs at both radar and communication functions. These multi-objective metrics enable to evaluate jointly the performance of both functions, highlighting possible trade-offs and enabling to perform joint transmit power optimisation for both RSUs and vehicles. Upper and lower bounds are also proposed. Finally, conditional metrics are defined from the joint metrics, namely (i) the coverage probability for vehicles already achieving a given detection or success probability, and (ii) the detection or success probability for vehicles already achieving a given coverage probability.
- All the proposed metrics are generalised to include Interference Cancellation (IC) capabilities at the radar and communication functions when they cooperate with each other. Either perfect IC is achieved, or partial cancellation is considered. The proposed framework works can integrate any residual interference function, depending of the radar and communication power levels. Further extensions and generalisations are also discussed.

C. Notations

In this paper, the probability and expectation operators are denoted $\mathbb{P}(\cdot)$ and $\mathbb{E}[\cdot]$. When the probability (resp. expectation) is computed over a specific random variable X, it is denoted $\mathbb{P}_X(\cdot)$ (resp. $\mathbb{E}_X[\cdot]$). When it is conditioned over a random variable or event Y, it is denoted either $\mathbb{P}_{\cdot|Y}(\cdot)$ (resp. $\mathbb{E}_{\cdot|Y}[\cdot]$) or $\mathbb{P}(\cdot|Y)$ (resp. $\mathbb{E}[\cdot|Y]$). The indicator function is denoted $\mathbb{1}$. The function Q_1 is the first order Marcum Q-function [33]. For a function g and a region $A \subseteq \mathbb{R}^n$, we define the operator

$$\mathcal{E}_A[g(\mathbf{X})] = \mathbb{E}_{\mathbf{X}}[g(\mathbf{X}) \cdot \mathbb{1}(\mathbf{X} \in A)],$$

with $\mathbf{X} \in \mathbb{R}^n$ a vector of random variables. It enables to compute the expectation over an arbitrary domain. We also

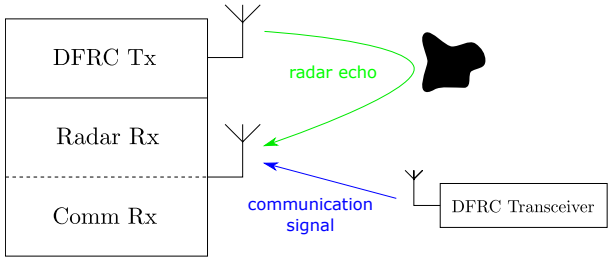


Fig. 1. Considered signals at the typical node. The communication signal (resp. radar echo) is considered as an interference for the radar (resp. communication) function.

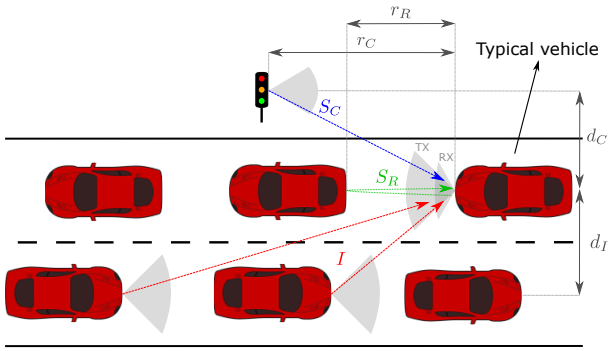


Fig. 2. Two-lane road scenario.

define an operator for two functions $g_1(s) \equiv g_1(s, \mathbf{X})$ and $g_2(s) \equiv g_2(s, \mathbf{X})$:

$$\mathcal{G}\left(g_1, g_2; A\right) = \mathcal{E}_A\left[\frac{1}{2} - \frac{1}{\pi}\int_0^\infty \frac{1}{\tau}\,\mathrm{Im}\left\{g_1(-j\tau)\,g_2(-j\tau)\right\}\mathrm{d}\tau\right].$$

It is used later to represent metrics evaluated using the Gil-Pelaez theorem [34].

D. Structure of the paper

The paper is structured as follows: First, the system model is detailed in Section II. Next, performance metrics are presented and developed in Section III. Then, the numerical analysis is performed in Section IV. Finally, the proposed framework is extended in Section V to include IC and multiple lanes. Other generalisations are discussed in Section VI.

II. System Model

A. Considered scenario

We consider a two-lane road scenario, as illustrated in Figure 2. The vehicles are equipped at the front side with a DFRC system. Their transmit power, transmit antenna beamwidth and receive antenna beamwidth are respectively denoted as P_V, ϕ_{VT} and ϕ_{VR}. The typical vehicle simultaneously receives a radar echo coming from the first vehicle in front driving in the same lane, and a communication signal from the nearest RSU ahead. The transmit power and transmit antenna beamwidth of this RSU are respectively denoted as P_L and ϕ_{LT}. The distance perpendicular to the road direction between the typical vehicle and the RSU (resp. the center of the opposite lane) is denoted d_C (resp. d_I). The echoes arising from vehicles driving in the opposite direction are not considered in this work. This assumption is motivated by the stronger attenuation affecting the radar echoes compared to the interfering signals, and the use of directive beamforming at the transmitter. IC of the interfering echoes at the communication function based on the acquired radar information could also be implemented, but this is out of the scope of this paper.

Assuming that the typical vehicle is located at $r = 0$, vehicles driving in the direction of the typical vehicle, interfering vehicles on the opposite way, and the RSUs are distributed on three parallel lines following three independent PPPs $\mathbf{\Phi}_R$, $\mathbf{\Phi}_I$ and $\mathbf{\Phi}_C$ of intensities respectively given by

$$\begin{aligned}\lambda_R(r) &= \lambda_R\,\mathbb{1}\left(r_{R\mathrm{min}} \le r \le r_{R\mathrm{max}}\right),\\ \lambda_I(r) &= \lambda_I\,\mathbb{1}\left(r_{I\mathrm{min}} \le r\right),\\ \lambda_C(r) &= \lambda_C\,\mathbb{1}\left(r_{C\mathrm{min}} \le r\right),\end{aligned} \tag{1}$$

where λ_R, λ_I and λ_C are respectively the densities of vehicles driving on the same lane as the typical vehicle, interfering vehicles and RSUs. The minimum and maximum detectable range of the radar function, the minimum distance (parallel to the road) of the communication signal and the minimum distance (parallel to the road) of the interfering signals are respectively denoted by $r_{R\mathrm{min}}$, $r_{R\mathrm{max}}$, $r_{C\mathrm{min}}$ and $r_{I\mathrm{min}}$. Note that $r_{C\mathrm{min}}$ and $r_{I\mathrm{min}}$ are directly related to the antenna beamwidths of the different systems: $r_{C\mathrm{min}} = d_C/\tan(\min(\phi_{\mathrm{LT}}, \phi_{\mathrm{VR}})/2)$ and $r_{I\mathrm{min}} = d_I/\tan(\min(\phi_{\mathrm{VT}}, \phi_{\mathrm{VR}})/2)$. PPPs have been chosen to model the node locations. The generalisation of the model with other point processes is nonetheless discussed in Section VI-A.

B. Propagation models

A linear path-loss model is considered with $[L_k(r)]_{\mathrm{dB}} = [\beta_k]_{\mathrm{dB}} + 10\alpha_k\,\log_{10}(r)$, where $k \in \{R, C, I\}$ designates the considered link, α_k is the path-loss exponent and β_k is the intercept. The received power for the communication link is given by the Friis equation [35] as

$$\begin{aligned}S_C(r) &= P_L G_C \frac{c^2}{4\pi f_c^2} L_C^{-1}\left(\sqrt{r^2 + d_C^2}\right)\\ &= \rho_C\left(r^2 + d_C^2\right)^{-\frac{\alpha_C}{2}},\end{aligned} \tag{2}$$

where r is the distance between the two nodes parallel to the road, and $\rho_C = \frac{P_L G_C c^2}{4\pi f_c^2 \beta_C}$. The speed of light is denoted by c, the carrier frequency by f_c, and G_C is the beamforming gain of the communication link. The interfering power is obtained in the same manner:

$$\begin{aligned}I &= \sum_{i\,|\,x_i \in \mathbf{\Phi}_I} P_V G_I \frac{c^2}{4\pi f_c^2} L_I^{-1}\left(\sqrt{x_i^2 + d_I^2}\right)|h_i|^2\\ &= \sum_{i\,|\,x_i \in \mathbf{\Phi}_I} \rho_I\left(x_i^2 + d_I^2\right)^{-\frac{\alpha_I}{2}}|h_i|^2,\end{aligned} \tag{3}$$

where $\rho_I = \frac{P_V G_I c^2}{4\pi f_c^2 \beta_I}$. The beamforming gain of the interfering links is denoted by G_I, and $|h_i|^2$ are i.i.d. rician distributed small-scale fading random variables. Note that the small-scale fading has been neglected in the communication link for the sake of tractability. However, it is assumed to be highly rician

since the RSU is located on the same side of the road (and not in the traffic as the interfering links), and high frequencies (24/77GHz) are considered for this application.

In the literature, the received power for the radar link is usually given by the radar equation [36]:

$$S_{R,\text{RCS}}(r) = P_V G_R \frac{c^2}{4\pi f_c^2} L_R^{-2}(r)\,\sigma, \tag{4}$$

with a distance r between the radar and the target, where σ is the RCS of the target, and G_R is the beamforming gain of the radar link. The RCS is often modelled as an exponentially distributed random variable, following the Swerling I model [37]. However, this model is valid in far field, i.e. when $r \geq \frac{2D^2 f_c}{c}$ with D the largest dimension of the reflector. To alleviate this issue, we instead modelled the received power for the radar link as

$$S_R(r) = P_V G_R \frac{c^2}{4\pi f_c^2} L_R^{-1}(2r) = \rho_R\, r^{-\alpha_R}, \tag{5}$$

with a distance r between the radar and the target. This model is valid for reflector dimensions larger than the first Fresnel zones diameter, namely $D \geq \sqrt{\frac{rc}{f_c}} \approx 25$ or 14cm at a distance of 5m, and carrier frequencies of 24 and 77GHz. Therefore, it is suited for the considered automotive scenario. Again, the small-scale fading is neglected for tractability, but it is also supposed to be highly rician considering the scenario and the high frequencies used in automotive radar applications.

To simplify the notations, we define $S_R \equiv S_R(r_R)$ where r_R is the distance between the vehicle of interest and the vehicle driving ahead, and $S_C \equiv S_C(r_C)$, where r_C is the distance (parallel to the road) between the vehicle of interest and the nearest RSU ahead. We also define $S_{R\text{min}} = S_R(r_{R\text{max}})$, $S_{R\text{max}} = S_R(r_{R\text{min}})$ and $S_{C\text{max}} = S_C(r_{C\text{min}})$ as the minimum and maximum possible power levels for the radar and communication links.

III. Development of the Metrics

Figure 3 illustrates the different metrics which are developed in this section. First, preliminary results enabling to compute all the metrics are obtained in Sections III-A and III-B. Then, in Sections III-C to III-E, the multiple single-objective metrics for radar and communication applications (i.e. the coverage probability, the false alarm probability, the detection probability and the success probability) are computed in the considered automotive scenario. Next, the new joint metrics (i.e. the JRDCCP and JRSCCP) are presented and developed in Sections III-F and III-G. Finally, upper and lower bounds for the single-objective metrics are obtained in Section III-H, and conditional metrics are developed in Section III-I.

A. Probability density functions of S_R and S_C

Knowing the statistics of the radar and communication powers S_R and S_C, averaging can be performed in order to express the metrics as a function of the (complementary) CDF of the interfering power I. The expressions of the PDFs of S_R and S_C are developed in Lemma 1.

Lemma 1: *Assuming that there is at least one vehicle in the radar detectable range, the PDFs of the radar and communication powers S_R and S_C are respectively given by*

$$f_{S_R}(s) = \frac{r_R(s)}{\alpha_R\, s} \frac{\lambda_R \exp\left(-\lambda_R(r_R(s) - r_{R\text{min}})\right)}{1 - \exp\left(-\lambda_R(r_{R\text{max}} - r_{R\text{min}})\right)} \cdot \mathbb{1}\left(S_{R\text{min}} \leq s \leq S_{R\text{max}}\right), \tag{6}$$

with $r_R(s) = \rho_R^{\frac{1}{\alpha_R}}\, s^{-\frac{1}{\alpha_R}}$ *, and*

$$f_{S_C}(s) = \frac{r_C^2(s) + d_C^2}{\alpha_C\, s\, r_C(s)} \lambda_C \exp\left(-\lambda_C(r_C(s) - r_{C\text{min}})\right) \cdot \mathbb{1}\left(0 \leq s \leq S_{C\text{max}}\right), \tag{7}$$

with $r_C(s) = \sqrt{\rho_C^{\frac{2}{\alpha_C}}\, s^{-\frac{2}{\alpha_C}} - d_C^2}$.

Proof: These results are obtained by applying a scalar-to-scalar change of variable with the PDFs of the distances r_R and r_C. Those are computed following the developments presented in [38], in one dimension. ■

B. Laplace transform of the interfering power I

Using Lemma 1, the different metrics are computed as a function of the (complementary) CDF of the interfering power I. Moreover, the Gil-Pelaez theorem [34] enables to compute this CDF based on its LT, which is obtained in Lemma 2.

Lemma 2: *The Laplace transform of the interfering power I is given by*

$$\mathcal{L}_I(s) = \exp\left(-\lambda_I \int_{r_{I\text{min}}}^{\infty} \left(1 - \mathcal{L}_{|h_i|^2}\left(s\chi(r)\right)\right) \mathrm{d}r\right), \tag{8}$$

where $\chi(r) = \rho_I \left(r^2 + d_I^2\right)^{-\frac{\alpha_I}{2}}$*, and* $\mathcal{L}_{|h_i|^2}$ *denotes the Laplace transform of the small-scale fading for the interfering links. Under rician fading, it is computed as*

$$\mathcal{L}_{|h_i|^2}(s) = \frac{K+1}{K+1+s} \exp\left(-\frac{Ks}{K+1+s}\right), \tag{9}$$

with K the rician K-factor of the interfering links.

Proof: This result is obtained applying the probability generating functional of a PPP, as done in [39], in one dimension. The LT of the small-scale fading is given in [40]. ■

C. Coverage probability

The *coverage probability* is defined as the probability to achieve a sufficient SINR for the communication function. The SINR threshold θ is set w.r.t. the achievable communication capacity requirement, given by $B\log_2(1+\theta)$ where B is the bandwidth of the transmission. For example, a threshold of 0dB corresponds to a capacity of 100Mbps with a bandwidth of 100MHz. It can also be set regarding a given Bit Error Rate (BER) requirement. For instance, a BER of 10^{-3} is achieved for a threshold of 9.8dB with a 4-QAM transmission over an AWGN channel.

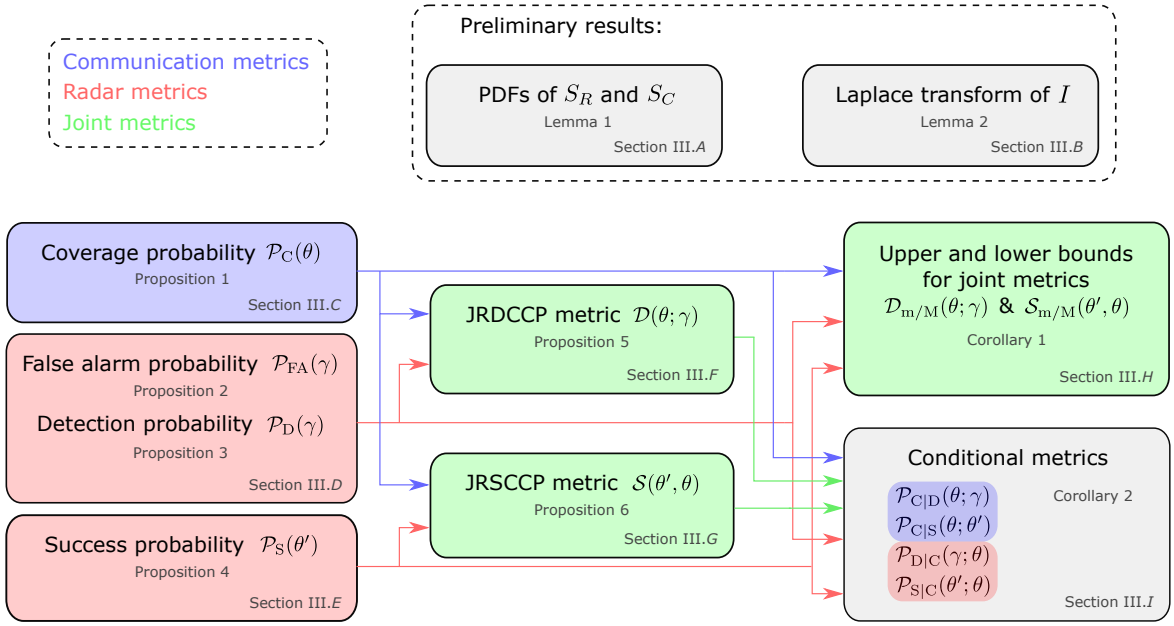


Fig. 3. Preliminary results and metrics obtained in Section III. Arrows represent relations between the metrics.

In the considered scenario, the radar echo from the next vehicle ahead and the signals coming from the vehicles on the opposite lane are interfering with the communication function. Assuming that the scenario is interference-limited, this metric is written as

$$\mathcal{P}_{\mathrm{C}}(\theta) = \mathbb{P}\left(\frac{S_C}{S_R + I} \geq \theta\right). \tag{10}$$

Proposition 1 gives the expression of the coverage probability depending on the required communication Signal to Interference Ratio (SIR) threshold θ.

Proposition 1: *For a given communication SIR threshold θ, the coverage probability is obtained as*

$$\mathcal{P}_{\mathrm{C}}(\theta) = \mathcal{G}\left(\mathcal{L}_I, \xi_C; \Xi_C\right), \tag{11}$$

where ξ_C and Ξ_C are defined in the second column of Table I. The operator $\mathcal{G}$ is defined in Section I-C.

Proof: The proof is detailed in Appendix A. ■

Note that the complementary CDF of the *spectral efficiency* can be computed based on the coverage probability:

$$\mathcal{R}(\eta) = \mathbb{P}\left(\log_2\left(1 + \frac{S_C}{S_R + I}\right) \geq \eta\right) = \mathcal{P}_{\mathrm{C}}\left(2^\eta - 1\right). \tag{12}$$

Similarly, the average spectral efficiency is computed as

$$\bar{\mathcal{R}} = \int_0^\infty \mathcal{R}(\eta)\,\mathrm{d}\eta = \frac{1}{\ln 2}\int_0^\infty \frac{\mathcal{P}_{\mathrm{C}}(\theta)}{1+\theta}\,\mathrm{d}\theta, \tag{13}$$

by applying the change of variable $\theta = 2^\eta - 1$.

D. Detection and false alarm probabilities

Let us consider the output of the radar receiver before the detector. As done in [36], two hypotheses are defined for each cell, i.e. each value of the delay-Doppler-angle map computed at its output:

- H_0 : there is no target within the cell;
- H_1 : there is a target within the cell.

The amplitude of the cell under test is described as

$$x = \begin{cases} A + w & \text{under } H_1, \\ w & \text{under } H_0, \end{cases} \tag{14}$$

where $A^2 = S_R\kappa$ with a radar processing gain κ, w is an Additive White Gaussian Noise (AWGN) of variance σ_w^2 modelling the noise and the interference. For a given threshold γ, the *false alarm probability* P_{FA} and *detection probability* P_{D} are respectively defined as

$$P_{\mathrm{FA}}(\gamma) = \mathbb{P}\left(|x|^2 \geq \gamma \,|\, H_0\right), \tag{15}$$
$$P_{\mathrm{D}}(\gamma) = \mathbb{P}\left(|x|^2 \geq \gamma \,|\, H_1\right). \tag{16}$$

In practice, a given false alarm probability is required, and the threshold is defined to meet this requirement.

In the considered automotive scenario, assuming that the scenario is interference-limited, these metrics are respectively rewritten as follows:

$$\mathcal{P}_{\mathrm{FA}}(\gamma) = \mathbb{P}\left(S_C + I \geq \gamma\right), \tag{17}$$
$$\mathcal{P}_{\mathrm{D}}(\gamma) = \mathbb{P}\left(S_R\kappa + S_C + I \geq \gamma\right). \tag{18}$$

Propositions 2 and 3 provide expressions of the false alarm and detection probabilities depending on the threshold of the radar detector γ.

Proposition 2: *For a given threshold γ, the false alarm probability is given by*

$$\mathcal{P}_{\mathrm{FA}}(\gamma) = 1 - \mathcal{G}\left(\mathcal{L}_I, \xi_F; \Xi_F\right), \tag{19}$$

where ξ_F and Ξ_F are defined in the second column of Table I.

Proof: The proof is detailed in Appendix B. ■

Proposition 3: *For a given threshold γ, the detection probability is given by*

$$\mathcal{P}_{\mathrm{D}}(\gamma) = 1 - \mathcal{G}\left(\mathcal{L}_I, \xi_D; \Xi_D\right), \tag{20}$$

with ξ_D and Ξ_D defined in the second column of Table I.

Proof: The proof is detailed in Appendix B. ■

E. Success probability

Following the hypothesis testing problem presented in Section III-D, for a given false alarm probability P_{FA}, the detection probability is given in [36] by

$$P_{\mathrm{D}} = Q_1\left(\sqrt{2A^2/\sigma_w^2}, \sqrt{-2\ln P_{\mathrm{FA}}}\right). \tag{21}$$

Therefore, since an increase of the radar SINR leads to a higher detection probability, the *success probability* has been defined as

$$P_{\mathrm{S}}(\theta') = \mathbb{P}\left(A^2/\sigma_w^2 \geq \theta'\right) \tag{22}$$

where θ' is a given radar SINR threshold. For a given false alarm requirement, the threshold θ' is set depending on the required detection probability. For example, [36, Figure 6.7] illustrates that a detection probability of 60% is achieved with a false alarm requirement of 10^{-4} for a radar SINR threshold of 10dB. Note that, similarly to the communication SINR threshold θ, it can also be set to ensure a given radar estimation rate [41].

In the considered automotive scenario, the nearest RSU ahead and the vehicles on the opposite lane interfere with the radar function. Assuming that the scenario is interference-limited, this metric is rewritten as follows:

$$\mathcal{P}_{\mathrm{S}}(\theta') = \mathbb{P}\left(\frac{S_R\kappa}{S_C + I} \geq \theta'\right). \tag{23}$$

Proposition 4 gives the expression of the success probability depending on the required radar SIR threshold θ'.

Proposition 4: *For a given radar SIR threshold θ', the success probability is obtained as*

$$\mathcal{P}_{\mathrm{S}}(\theta') = \mathcal{G}\left(\mathcal{L}_I, \xi_S; \Xi_S\right), \tag{24}$$

where ξ_S and Ξ_S are defined in the second column of Table I.

Proof: The proof is detailed in Appendix A. ■

F. JRDCCP metric

We define the Joint Radar Detection and Communication Coverage Probability (JRDCCP) as an extension of the communication coverage and the radar detection probabilities for joint radar-communication scenarios:

$$\mathcal{D}(\theta;\gamma) = \mathbb{P}\left(S_R\kappa + S_C + I \geq \gamma,\ \frac{S_C}{S_R + I} \geq \theta\right) \tag{25}$$

for a given $\mathcal{P}_{\mathrm{FA}}(\gamma)$.

It gives the probability that a radar detection occurs for a given false alarm probability, while ensuring a sufficient SIR for the communication function. The threshold γ is selected in order to fulfill the false alarm probability requirement, and the JRDCCP metric is then obtained for a given communication SIR threshold θ. The metric is developed in Proposition 5.

Proposition 5: *For a given communication SIR threshold θ and a given false alarm probability $\mathcal{P}_{FA}$ (or equivalently a given threshold γ), the JRDCCP metric is obtained as*

$$\mathcal{D}(\theta;\gamma) = \mathcal{G}\left(\mathcal{L}_I, \psi_{\mathrm{D1}}; \Omega_{\mathrm{D1}}\right) + \mathcal{G}\left(\mathcal{L}_I, \psi_{\mathrm{D2}}; \Omega_{\mathrm{D2}}\right) - \mathcal{E}_{\Omega_{\mathrm{D2}}}\left[\frac{1}{2}\right], \tag{26}$$

where ψ_{D1}, ψ_{D2}, Ω_{D1} and Ω_{D2} are defined in the second column of Table I.

Proof: The proof is detailed in Appendix B. ■

G. JRSCCP metric

We define the Joint Radar Success and Communication Coverage Probability (JRSCCP) as an extension of the success probability for joint radar-communication scenarios:

$$\mathcal{S}(\theta',\theta) = \mathbb{P}\left(\frac{S_R\kappa}{S_C + I} \geq \theta',\ \frac{S_C}{S_R + I} \geq \theta\right). \tag{27}$$

It gives the probability that both the radar and communication SIRs are sufficient compared to the threshold requirements. This metric is developed in Proposition 6.

Proposition 6: *For a given radar SIR threshold θ' and communication SIR threshold θ, if the following condition is fulfilled:*

$$[\theta']_{\mathrm{dB}} + [\theta]_{\mathrm{dB}} \leq [\kappa]_{\mathrm{dB}}, \tag{28}$$

the JRSCCP metric is obtained as

$$\mathcal{S}(\theta',\theta) = \mathcal{G}\left(\mathcal{L}_I, \psi_{\mathrm{S1}}; \Omega_{\mathrm{S1}}\right) + \mathcal{G}\left(\mathcal{L}_I, \psi_{\mathrm{S2}}; \Omega_{\mathrm{S2}}\right), \tag{29}$$

where ψ_{S1}, ψ_{S2}, Ω_{S1} and Ω_{S2} are defined in the second column of Table I. Otherwise, the metric is equal to zero.

Proof: The proof is detailed in Appendix A. ■

H. Upper and lower bounds

Using Fréchet inequalities [42], upper and lower bounds are proposed for both joint metrics in Corollary 1.

Corollary 1: *For a given communication SIR threshold θ and a given false alarm probability $\mathcal{P}_{FA}$ (or equivalently a given threshold γ), the JRDCCP metric is bounded by*

$$\mathcal{D}_{\mathrm{m}}(\theta;\gamma) \leq \mathcal{D}(\theta;\gamma) \leq \mathcal{D}_{\mathrm{M}}(\theta;\gamma), \tag{30}$$

with

$$\mathcal{D}_{\mathrm{m}}(\theta;\gamma) = \max\left(0, \mathcal{P}_{\mathrm{D}}(\gamma) + \mathcal{P}_{\mathrm{C}}(\theta) - 1\right), \tag{31}$$

$$\mathcal{D}_{\mathrm{M}}(\theta;\gamma) = \min\left(\mathcal{P}_{\mathrm{D}}(\gamma), \mathcal{P}_{\mathrm{C}}(\theta)\right). \tag{32}$$

Similarly, for a given radar SIR threshold θ' and communication SIR threshold θ, the JRSCCP metric is bounded by

$$\mathcal{S}_{\mathrm{m}}(\theta',\theta) \leq \mathcal{S}(\theta',\theta) \leq \mathcal{S}_{\mathrm{M}}(\theta',\theta), \tag{33}$$

TABLE I

FUNCTIONS AND REGIONS OF INTEGRATION FOR THE DIFFERENT METRICS, WITHOUT (SECTION III) AND WITH (SECTION V-A) IC CAPABILITIES.

Metric	Without IC (Section III)		With IC (Section V-A)	
	Function ξ/ψ	Region Ξ/Ω	Function ξ/ψ	Region Ξ/Ω
Coverage prob. $\mathcal{P}_{\mathrm{C}}$	$\xi_C(s) = \exp\left(s\left(\frac{S_C}{\theta} - S_R\right)\right)$	$\Xi_C \triangleq \begin{Bmatrix} S_{R\min} \leq S_R \leq S_{R\max} \\ \theta S_R \leq S_C \leq S_{C\max} \end{Bmatrix}$	$\xi_C^{\mathrm{IC}}(s) = \exp\left(s\left(\frac{S_C}{\theta} - \zeta_R\right)\right)$	$\Xi_C^{\mathrm{IC}} \triangleq \begin{Bmatrix} S_C - \theta\zeta_R \geq 0 \\ S_{R\min} \leq S_R \leq S_{R\max} \\ 0 \leq S_C \leq S_{C\max} \end{Bmatrix}$
False alarm prob. $\mathcal{P}_{\mathrm{FA}}$	$\xi_F(s) = \exp\left(s(\gamma - S_C)\right)$	$\Xi_F \triangleq \begin{Bmatrix} S_C \leq \gamma \\ 0 \leq S_C \leq S_{C\max} \end{Bmatrix}$	$\xi_F^{\mathrm{IC}}(s) = \exp\left(s(\gamma - \zeta_C)\right)$	$\Xi_F^{\mathrm{IC}} \triangleq \begin{Bmatrix} \zeta_C \leq \gamma \\ S_{R\min} \leq S_R \leq S_{R\max} \\ 0 \leq S_C \leq S_{C\max} \end{Bmatrix}$
Detection prob. $\mathcal{P}_{\mathrm{D}}$	$\xi_D(s) = \exp\left(s(\gamma - S_R\kappa - S_C)\right)$	$\Xi_D \triangleq \begin{Bmatrix} S_C \leq \gamma - S_R\kappa \\ S_{R\min} \leq S_R \leq S_{R\max} \\ 0 \leq S_C \leq S_{C\max} \end{Bmatrix}$	$\xi_D^{\mathrm{IC}}(s) = \exp\left(s(\gamma - S_R\kappa - \zeta_C)\right)$	$\Xi_D^{\mathrm{IC}} \triangleq \begin{Bmatrix} \gamma - S_R\kappa - \zeta_C \geq 0 \\ S_{R\min} \leq S_R \leq S_{R\max} \\ 0 \leq S_C \leq S_{C\max} \end{Bmatrix}$
Success prob. $\mathcal{P}_{\mathrm{S}}$	$\xi_S(s) = \exp\left(s\left(\frac{S_R\kappa}{\theta'} - S_C\right)\right)$	$\Xi_S \triangleq \begin{Bmatrix} S_C \leq S_R\kappa/\theta' \\ S_{R\min} \leq S_R \leq S_{R\max} \\ 0 \leq S_C \leq S_{C\max} \end{Bmatrix}$	$\xi_S^{\mathrm{IC}}(s) = \exp\left(s\left(\frac{S_R\kappa}{\theta'} - \zeta_C\right)\right)$	$\Xi_S^{\mathrm{IC}} \triangleq \begin{Bmatrix} \zeta_C \leq S_R\kappa/\theta' \\ S_{R\min} \leq S_R \leq S_{R\max} \\ 0 \leq S_C \leq S_{C\max} \end{Bmatrix}$
JRDCCP $\mathcal{D}$	$\psi_{\mathrm{D1}}(s) = \xi_C(s)$	$\Omega_{\mathrm{D1}} \triangleq \begin{Bmatrix} S_C \geq \max\left(\theta S_R, \gamma - S_R\kappa\right) \\ S_{R\min} \leq S_R \leq S_{R\max} \\ 0 \leq S_C \leq S_{C\max} \end{Bmatrix}$	$\psi_{\mathrm{D1}}^{\mathrm{IC}}(s) = \xi_C^{\mathrm{IC}}(s)$	$\Omega_{\mathrm{D1}}^{\mathrm{IC}} \triangleq \begin{Bmatrix} \gamma - S_R\kappa - \zeta_C \leq 0 \\ \frac{S_C}{\theta} - \zeta_R \geq 0 \\ S_{R\min} \leq S_R \leq S_{R\max} \\ 0 \leq S_C \leq S_{C\max} \end{Bmatrix}$
	$\psi_{\mathrm{D2}}(s) = \xi_C(s) - \xi_D(s)$	$\Omega_{\mathrm{D2}} \triangleq \begin{Bmatrix} \frac{\theta\gamma}{\theta+1} - S_R\frac{\theta(\kappa-1)}{\theta+1} \leq S_C \leq \gamma - \kappa S_R \\ S_{R\min} \leq S_R \leq S_{R\max} \\ 0 \leq S_C \leq S_{C\max} \end{Bmatrix}$	$\psi_{\mathrm{D2}}^{\mathrm{IC}}(s) = \xi_C^{\mathrm{IC}}(s) - \xi_D^{\mathrm{IC}}(s)$	$\Omega_{\mathrm{D2}}^{\mathrm{IC}} \triangleq \begin{Bmatrix} \gamma - S_R\kappa - \zeta_C \geq 0 \\ \frac{S_C}{\theta} - \zeta_R \geq \gamma - S_R\kappa - \zeta_C \\ S_{R\min} \leq S_R \leq S_{R\max} \\ 0 \leq S_C \leq S_{C\max} \end{Bmatrix}$
JRSCCP $\mathcal{S}$	$\psi_{\mathrm{S1}}(s) = \xi_S(s)$	$\Omega_{\mathrm{S1}} \triangleq \begin{Bmatrix} S_R\frac{\theta(\theta'+\kappa)}{\theta'(\theta+1)} \leq S_C \leq \frac{S_R\kappa}{\theta'} \\ S_{R\min} \leq S_R \leq S_{R\max} \\ 0 \leq S_C \leq S_{C\max} \end{Bmatrix}$	$\psi_{\mathrm{S1}}^{\mathrm{IC}}(s) = \xi_S^{\mathrm{IC}}(s)$	$\Omega_{\mathrm{S1}}^{\mathrm{IC}} \triangleq \begin{Bmatrix} \frac{S_R\kappa}{\theta'} - \zeta_C \geq 0 \\ \frac{S_C}{\theta} - \zeta_R \geq \frac{S_R\kappa}{\theta'} - \zeta_C \\ S_{R\min} \leq S_R \leq S_{R\max} \\ 0 \leq S_C \leq S_{C\max} \end{Bmatrix}$
	$\psi_{\mathrm{S2}}(s) = \xi_C(s)$	$\Omega_{\mathrm{S2}} \triangleq \begin{Bmatrix} \theta S_R \leq S_C \leq S_R\frac{\theta(\theta'+\kappa)}{\theta'(\theta+1)} \\ S_{R\min} \leq S_R \leq S_{R\max} \\ 0 \leq S_C \leq S_{C\max} \end{Bmatrix}$	$\psi_{\mathrm{S2}}^{\mathrm{IC}}(s) = \xi_C^{\mathrm{IC}}(s)$	$\Omega_{\mathrm{S2}}^{\mathrm{IC}} \triangleq \begin{Bmatrix} \frac{S_C}{\theta} - \zeta_R \geq 0 \\ \frac{S_R\kappa}{\theta'} - \zeta_C \geq \frac{S_C}{\theta} - \zeta_R \\ S_{R\min} \leq S_R \leq S_{R\max} \\ 0 \leq S_C \leq S_{C\max} \end{Bmatrix}$

with

$$\mathcal{S}_{\mathrm{m}}(\theta', \theta) = \max\left(0, \mathcal{P}_{\mathrm{S}}(\theta') + \mathcal{P}_{\mathrm{C}}(\theta) - 1\right), \tag{34}$$

$$\mathcal{S}_{\mathrm{M}}(\theta', \theta) = \min\left(\mathcal{P}_{\mathrm{S}}(\theta'), \mathcal{P}_{\mathrm{C}}(\theta)\right). \tag{35}$$

Proof: The proposed bounds are given by Fréchet inequalities. ■

I. Conditional metrics

One can be interested in the performance achieved by vehicles already fulfilling successfully one of the two functions. On the one hand, for the radar function, it is supposed that either a radar detection has occured, or that the radar SIR fulfills a given threshold requirement. Conditional metrics are then respectively expressed as follows:

$$\mathcal{P}_{\mathrm{C|D}}(\theta; \gamma) = \mathbb{P}\left(\frac{S_C}{S_R + I} \geq \theta \,\middle|\, S_R\kappa + S_C + I \geq \gamma\right) \tag{36}$$

for a given $\mathcal{P}_{\mathrm{FA}}(\gamma)$,

$$\mathcal{P}_{\mathrm{C|S}}(\theta; \theta') = \mathbb{P}\left(\frac{S_C}{S_R + I} \geq \theta \,\middle|\, \frac{S_R\kappa}{S_C + I} \geq \theta'\right). \tag{37}$$

On the other hand, for the communication function, it is supposed that the communication SIR fulfills a given threshold requirement. Conditional metrics are then expressed as follows:

$$\mathcal{P}_{\mathrm{D|C}}(\gamma; \theta) = \mathbb{P}\left(S_R\kappa + S_C + I \geq \gamma \,\middle|\, \frac{S_C}{S_R + I} \geq \theta\right) \tag{38}$$

for a given $\mathcal{P}_{\mathrm{FA}}(\gamma)$,

$$\mathcal{P}_{\mathrm{S|C}}(\theta'; \theta) = \mathbb{P}\left(\frac{S_R\kappa}{S_C + I} \geq \theta' \,\middle|\, \frac{S_C}{S_R + I} \geq \theta\right). \tag{39}$$

The different conditional metrics are detailed in Corollary 2.

Corollary 2: *For a given false alarm probability $\mathcal{P}_{FA}$ (and therefore for a given threshold γ) or a given radar SIR threshold θ', the coverage probabilities achieved by vehicles performing successfully the radar function for a given communication SIR threshold θ are given by*

$$\mathcal{P}_{\mathrm{C|D}}(\theta; \gamma) = \mathcal{D}(\theta; \gamma)/\mathcal{P}_{\mathrm{D}}(\gamma), \tag{40}$$

$$\mathcal{P}_{\mathrm{C|S}}(\theta; \theta') = \mathcal{S}(\theta', \theta)/\mathcal{P}_{\mathrm{S}}(\theta'). \tag{41}$$

Similarly, the detection and success probabilities achieved by vehicles performing successfully the communication function are given by

$$\mathcal{P}_{\mathrm{D|C}}(\gamma; \theta) = \mathcal{D}(\theta; \gamma)/\mathcal{P}_{\mathrm{C}}(\theta), \tag{42}$$

$$\mathcal{P}_{\mathrm{S|C}}(\theta'; \theta) = \mathcal{S}(\theta', \theta)/\mathcal{P}_{\mathrm{C}}(\theta). \tag{43}$$

Proof: These results are obtained using Bayes law. ■

Note that the average spectral efficiency can also be evaluated for these users following (13):

$$\bar{\mathcal{R}}_{|\mathrm{D}} = \frac{1}{\ln 2}\int_0^\infty \frac{\mathcal{P}_{\mathrm{C|D}}(x)}{1+x}\,\mathrm{d}x,\ \bar{\mathcal{R}}_{|\mathrm{S}} = \frac{1}{\ln 2}\int_0^\infty \frac{\mathcal{P}_{\mathrm{C|S}}(x)}{1+x}\,\mathrm{d}x.$$

IV. Numerical Analysis

In Section IV-A, the presented metrics are computed in a given scenario with parameters summarised in Table II. The validity of the analytical models is assessed through Monte-Carlo simulations. Additionally, joint power optimisation is performed using the JRSCCP metric in Section IV-B.

TABLE II
SCENARIO PARAMETERS.

$P_V = P_L = 20\mathrm{dBm}$	$G_R = G_C = G_I = 1$
$\kappa = 1$	$d_C = 2.5\mathrm{m}$, $d_I = 3\mathrm{m}$
$r_{R\mathrm{min}} = 5\mathrm{m}$, $\phi_{\mathrm{VT}} = 22.5°$, $\phi_{\mathrm{VR}} = \phi_{\mathrm{LT}} = 45°$	
$\lambda_V = 0.02\mathrm{m}^{-1}$, $\lambda_L = 0.01\mathrm{m}^{-1}$, $\lambda_I = 0.002\mathrm{m}^{-1}$	
$\beta_R = \beta_C = \beta_I = 4\pi$	$\alpha_R = 2$, $\alpha_C = \alpha_I = 3$

A. Metrics analysis

Figure 4 illustrates the false alarm probability, the detection probability and the JRDCCP metric, obtained with stochastic geometry and Monte-Carlo simulations. Following expressions in (17) and (18), the false alarm probability is always lower than the detection probability at any threshold. The false alarm and detection probabilities decrease to zero when the radar threshold increases. Therefore, the number of false alarms is lowered at the price of less detections.

For low values of the radar threshold γ (corresponding to high false alarm probabilities), the detection probability is close to one, and the JRDCCP metric tends to be equal to the communication coverage probability. Contrariwise, for low values of the communication SIR threshold θ, the communication coverage probability is close to one and the JRDCCP metric tends to be equal to the detection probability. The same behaviour is obtained with the JRSCCP metric, shown in Figure 5. For low values of the radar SIR threshold θ', the radar success probability is close to one and the JRSCCP tends to be equal to the coverage probability. By contrast, for low values of θ, the coverage probability is close to one, and the JRSCCP tends to be equal to the radar success probability. Additionally, the condition given in (28) is verified: with a radar processing gain set to one, whatever the values of θ' and θ, the metric decreases to zero when the sum (in dB) exceeds 0dB. This condition illustrates directly that a trade-off should be achieved between the radar and the communication function: owing to the negative impact of the communication signal on the radar function and vice-versa, arbitrarily high performance cannot be achieved simultaneously by both functions.

Two conditional metrics are also illustrated in Figure 5d, in which the same condition applies: among the vehicle achieving at least a communication (resp. radar) SIR θ (resp. θ') in dB, there is a zero probability of achieving a radar (resp. communication) SIR higher than -θ' (resp. -θ) in dB. This illustrates again a trade-off between the radar and the communication function: if an arbitrary requirement is given for one function, it is not possible to achieve arbitrarily high performance with the other function.

Upper and lower bounds are illustrated in both graphs for one curve (magenta). In both cases, the bounds become tighter as the joint metrics are evaluated for lower thresholds. In these cases, the joint metrics tend to be equal to radar or communication metrics (detection, success and coverage probabilities) and the bounds merge with the metrics.

B. Optimisation of the power levels

Using the joint metrics, optimisation w.r.t. the RSUs and vehicles transmit powers can be performed. With the JRSCCP metric, the optimisation problem is formulated for given radar and communication SIR thresholds θ' and θ as

$$\begin{aligned} {P_L}^*, {P_V}^* = \underset{P_L, P_V}{\arg\max}\quad & \mathcal{S}(\theta', \theta; P_L, P_V) \\ \text{s.t.}\quad & P_{L\mathrm{m}} \le P_L \le P_{L\mathrm{M}}, \\ & P_{V\mathrm{m}} \le P_V \le P_{V\mathrm{M}}. \end{aligned} \tag{44}$$

Minimum and maximum values for both RSUs and vehicles powers are respectively denoted by $P_{L\mathrm{m}}$, $P_{L\mathrm{M}}$, $P_{V\mathrm{m}}$ and $P_{V\mathrm{M}}$. With the JRDCCP metric, the optimisation problem is formulated similarly.

Figure 6 illustrates how the JRSCCP metric evolves for different transmit powers P_V and P_L at given SIR thresholds θ and θ'. Under the interference-limited scenario assumption, the JRSCCP metric can be expressed as a function of the ratio $\mu \equiv P_L/P_V$ between the RSUs and vehicles transmit powers. The power ratio should be therefore set such that neither the radar nor the communication function is disadvantaged, relatively to the required thresholds. Denoting by $\tilde{S}_R \equiv S_R/P_V$, $\tilde{S}_C \equiv S_C/P_L$, $\tilde{I} \equiv I/P_V$, (44) can be rewritten as

$$\begin{aligned} \mu^* = \underset{\mu}{\arg\max}\quad & \mathcal{S}(\theta', \theta; \mu) \\ \text{s.t.}\quad & \mu_{\mathrm{m}} \le \mu \le \mu_{\mathrm{M}}, \end{aligned} \tag{45}$$

with $\mu_{\mathrm{m}} = P_{L\mathrm{m}}/P_{V\mathrm{M}}$, $\mu_{\mathrm{M}} = P_{L\mathrm{M}}/P_{V\mathrm{m}}$, and

$$\mathcal{S}(\theta', \theta; \mu) = \mathbb{P}\left(\frac{\tilde{S}_R\kappa}{\mu\,\tilde{S}_C + \tilde{I}} \ge \theta',\ \mu\,\frac{\tilde{S}_C}{\tilde{S}_R + \tilde{I}} \ge \theta\right). \tag{46}$$

This enables in that case to perform univariate optimisation in order to solve (45), for instance with a one-dimensional grid search. When μ^* is found, one can select the lowest power levels satisfying $\mu^* = {P_L}^*/{P_V}^*$ and the power constraints.

The achieved JRSCCP metric after power optimisation is illustrated in Figure 7, for power levels between 0 and 60dBm. For each pair of SIR thresholds, the joint metric is optimised w.r.t. the RSUs and vehicles transmit powers, and the achieved performance is shown. As expected, the achieved performance is higher when low SIR thresholds are required. Condition (28) is again highlighting a trade-off between both functions: even with power optimisation, arbitrarily high requirements cannot be set for both functions simultaneously. The same

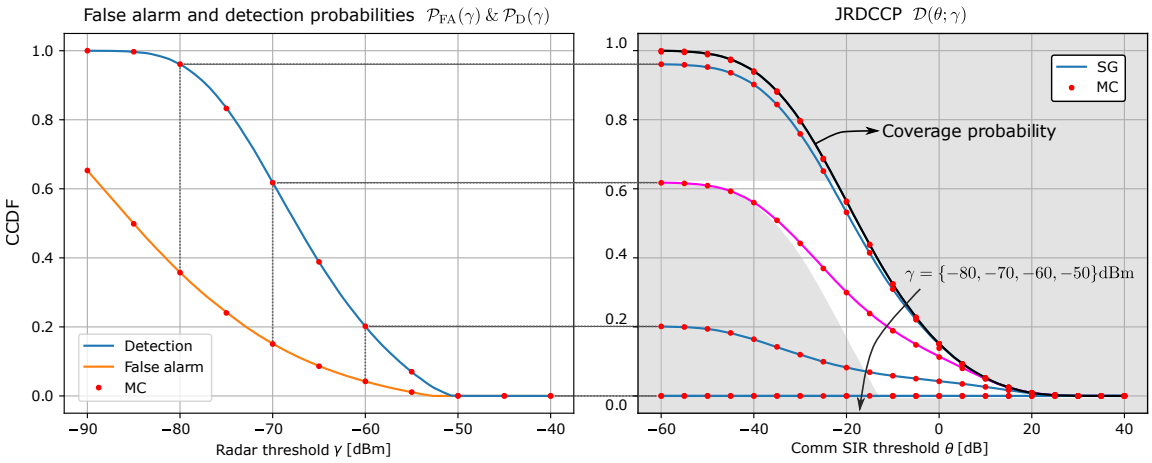


Fig. 4. False alarm probability, detection probability (left) and JRDCCP metric (right). The white area corresponds to the region delimited by the upper and lower bounds of the magenta curve.

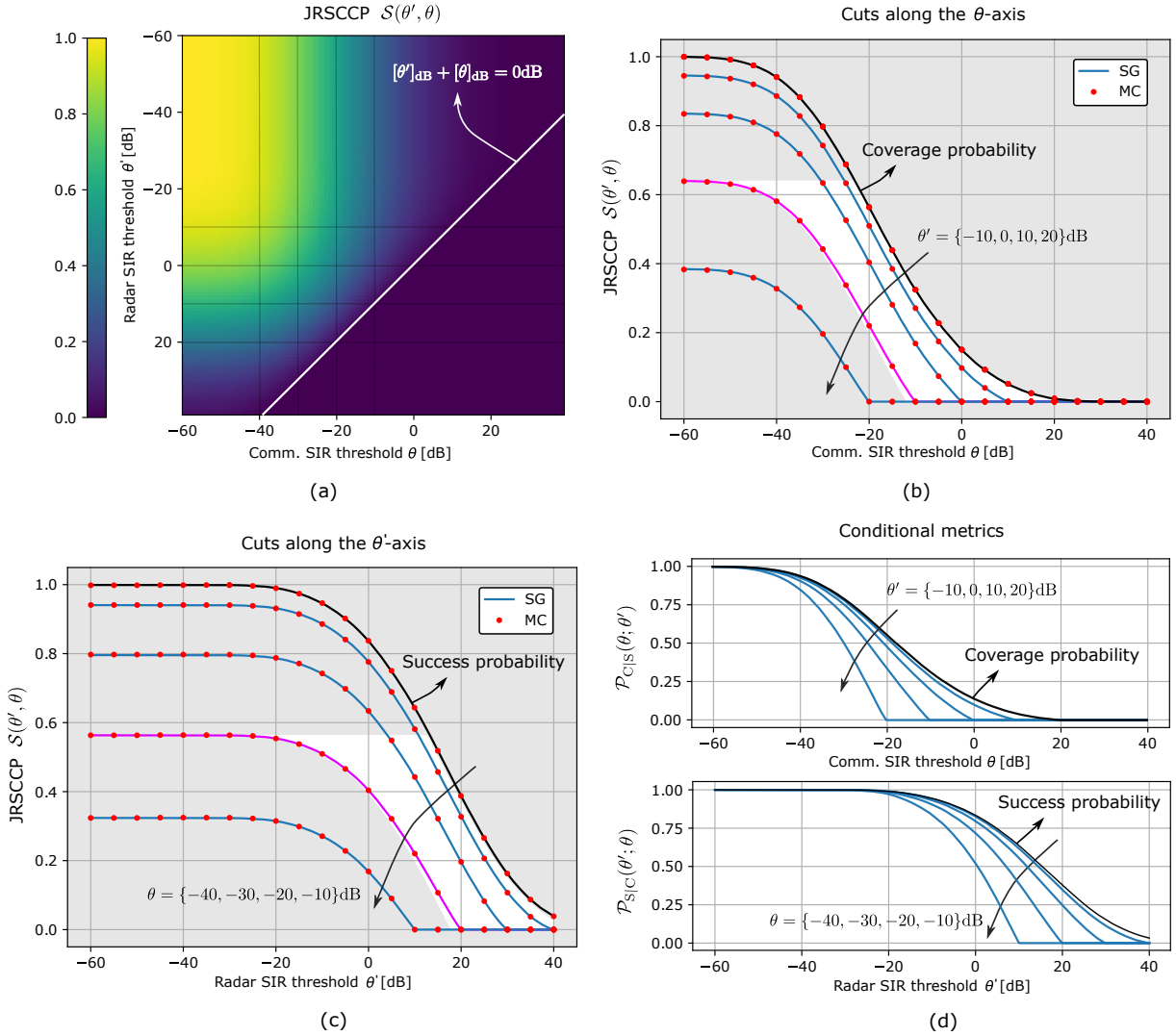


Fig. 5. JRSCCP metric (a), cut along the θ-axis (b), cut along the θ'-axis (c) and conditional metrics (d). The white areas in (b) and (c) correspond to the regions delimited by the upper and lower bounds of the magenta curves.

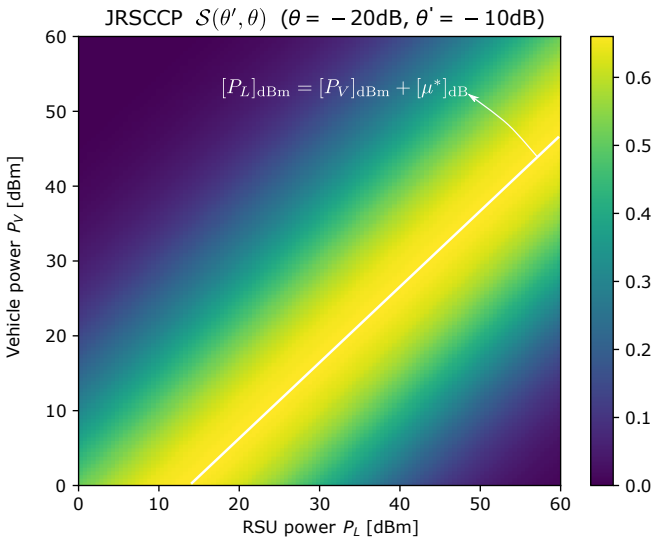


Fig. 6. JRSCCP vs transmitted powers, with $\theta' = -10$dB and $\theta = -20$dB. The optimal power ratio of (45) is denoted by μ^*.

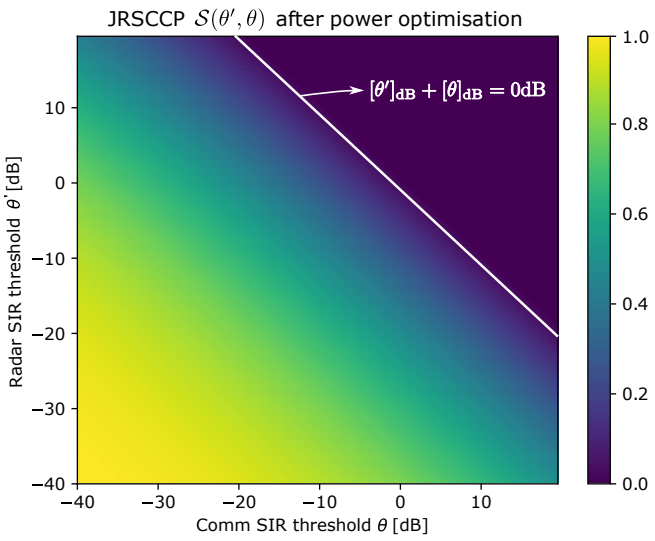


Fig. 7. JRSCCP for different radar and communication SIR thresholds θ' and θ, with RSUs and vehicles transmit powers optimised for each pair of thresholds. The minimum and maximum powers are $P_{L\text{m}} = P_{V\text{m}} = 0$dBm and $P_{L\text{M}} = P_{V\text{M}} = 60$dBm.

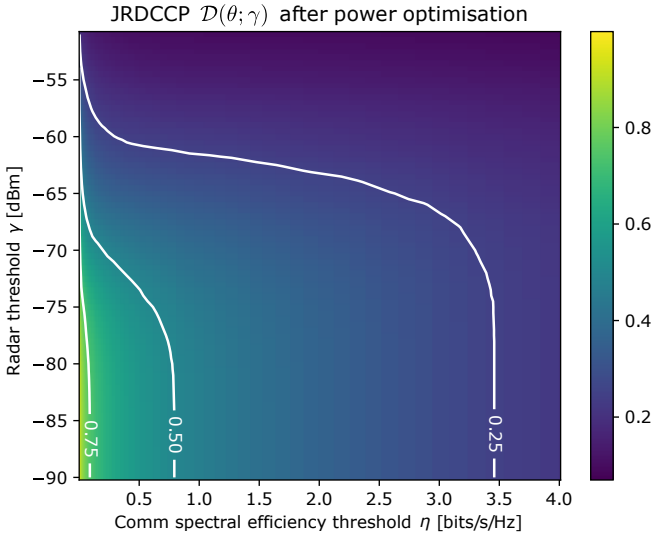


Fig. 8. JRDCCP for different radar thresholds γ and communication spectral efficiency thresholds $\eta = 2^{\theta} - 1$, with RSUs and vehicles transmit powers optimised for each pair of thresholds. The minimum and maximum powers are $P_{L\text{m}} = P_{V\text{m}} = 0$dBm and $P_{L\text{M}} = P_{V\text{M}} = 60$dBm.

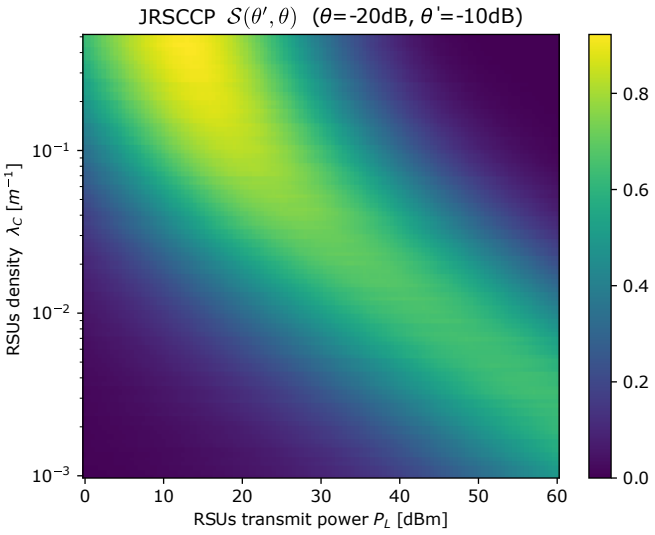


Fig. 9. JRSCCP vs RSUs transmitted power and density, with $\theta' = -10$dB and $\theta = -20$dB, and $P_V = 30$dBm.

is performed for the JRDCCP metric shown Figure 8, in which the change of variable of (12) has been performed to show the joint radar detection and communication spectral efficiency. Again, higher performance are reached for low radar thresholds γ, but low radar thresholds also induce higher false alarm probabilities. For the considered scenarios, radar thresholds up to -80dBm give similar performance, ensuring a communication rate of 0.8bits/s/Hz or higher in at least 50% of cases.

One can also be interested to optimise the RSU transmit power and density for a given vehicle transmit power and SIR thresholds. For instance, with the JRSCCP metric, the optimisation problem is formulated as

$$\begin{aligned} {P_L}^*, \lambda_C^* = \underset{P_L,\lambda_C}{\arg\max} \quad & \mathcal{S}(\theta',\theta;P_L,\lambda_C) \\ \text{s.t.} \quad & P_{L\text{m}} \leq P_L \leq P_{L\text{M}}, \\ & \lambda_{C\text{m}} \leq P_V \leq \lambda_{C\text{M}}. \end{aligned} \tag{47}$$

Minimum and maximum values for the RSU density are respectively denoted by $\lambda_{C\text{m}}$ and $\lambda_{C\text{M}}$. Similar conclusions are drawn, as shown in Figure 9, where the problem has been solved with a two-dimensional grid search: an increased density leads to a higher probability for the nearest RSU to be close. Therefore, the communication power is higher, increasing the communication SIR, but also the interference for the radar function. Additionally, increasing the density enables

to reduce the transmit power. Finally, better performance are achieved for high densities with low transmit power, instead of low densities with high transmit power.

V. System Model Extensions

A. Interference Cancellation

From the radar point of view, any communication signal arriving at the receiver is an interfering signal. From the communication point of view, any unwanted communication signal reaching the receiver is interfering, but the radar echo coming back to the DFRC transmitter is also considered as interference. Enabling some cooperation between both functions, communication signals which are decoded at the communication receiver could be (partially) suppressed at the radar receiver, and radar echoes which are processed at the radar receiver could be (partially) suppressed at the communication receiver. We assume that the signals coming from the interfering vehicles are not decoded by the typical vehicle. Therefore, the interference arising from the opposite lane is not cancelled, but the cooperation of both functions enables to mitigate the impact of S_R on the communication function, and S_C on the radar function. IC is modelled in [43] by multiplying the interference term by a chosen $\zeta \in [0,1]$. Perfect IC is achieved when $\zeta = 0$, while no IC is performed when $\zeta = 1$. Another approach is followed in [44], which defines the coverage probability as the probability to simultaneously have the interference-to-signal-plus-noise and the signal-to-noise ratio higher than a given SINR threshold. In this paper, we instead assume that the higher the SINR at the communication (resp. radar) receiver, the better the IC at the radar (resp. communication) receiver. Thus, the ζ factor depends on the performance of the decoding at the other function.

Denoting by $\zeta_R \equiv \zeta_R(S_R, S_C)$ and $\zeta_C \equiv \zeta_C(S_R, S_C)$ the residual interference after IC, the metrics presented in Sections III-C to III-G are respectively rewritten as

$$\mathcal{P}_{\mathrm{C}}^{\mathrm{IC}}(\theta) = \mathbb{P}\left(\frac{S_C}{\zeta_R + I} \geq \theta\right), \tag{48}$$

$$\mathcal{P}_{\mathrm{FA}}^{\mathrm{IC}}(\gamma) = \mathbb{P}\left(\zeta_C + I \geq \gamma\right), \tag{49}$$

$$\mathcal{P}_{\mathrm{D}}^{\mathrm{IC}}(\gamma) = \mathbb{P}\left(S_R\kappa + \zeta_C + I \geq \gamma\right), \tag{50}$$

$$\mathcal{P}_{\mathrm{S}}^{\mathrm{IC}}(\theta') = \mathbb{P}\left(\frac{S_R\kappa}{\zeta_C + I} \geq \theta'\right), \tag{51}$$

$$\mathcal{D}^{\mathrm{IC}}(\theta;\gamma) = \mathbb{P}\left(S_R\kappa + \zeta_C + I \geq \gamma,\ \frac{S_C}{\zeta_R + I} \geq \theta\right) \tag{52}$$

for a given $\mathcal{P}_{\mathrm{FA}}^{\mathrm{IC}}(\gamma)$,

$$\mathcal{S}^{\mathrm{IC}}(\theta',\theta) = \mathbb{P}\left(\frac{S_R\kappa}{\zeta_C + I} \geq \theta',\ \frac{S_C}{\zeta_R + I} \geq \theta\right). \tag{53}$$

The residual interference ζ_R is supposed to be high when the radar SIR is low since the radar receiver has difficulties to estimate correctly the delays and Doppler frequencies of the different targets. When this SIR is close to 0dB, the interference level could even be increased. Similarly, the same applies for ζ_C when the communication SIR is low since the communication receiver has difficulties to decode the communication signal and to estimate the channel parameters.

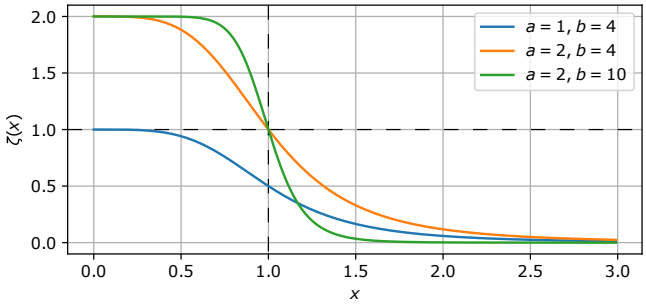


Fig. 10. Function of residuals $\zeta(x) = \frac{a}{1+x^b}$ for different parameters a and b.

Conversely, when these ratios are high, the interference is efficiently cancelled, leading to nearly zero residuals. For tractability, even if the total interference should be considered to assess the performance achieved by the IC scheme, we assume that these functions do not depend on the interfering signals I. In this paper, three different cases are evaluated.

1) No IC is performed:
$$\zeta_R = S_R, \quad \zeta_C = S_C, \tag{54}$$
leading back to definitions given in Section III.
2) An imperfect IC is performed at both functions simultaneously, leading to the following residuals:
$$\zeta_R = S_C\,\zeta\left(\frac{S_R}{S_C}\right), \quad \zeta_C = S_R\,\zeta\left(\frac{S_C}{S_R}\right). \tag{55}$$
The function $\zeta(x)$ should ideally describe how the IC scheme performs depending on the radar and communication power levels ratio x. In view of all the arguments set out above, following simulations of the interference cancellation schemes detailed in [45], we propose to define the function ζ in this paper as
$$\zeta(x) = \frac{a}{1+x^b}, \tag{56}$$
where a and b are two fitting parameters. This function is illustrated in Figure 10 for different values of a and b. With such function, for low power ratios, ζ is constant, and the residual interference increases proportionally with the power of the other function, since it dominates the received signal. In contrary, for high power ratios, $\zeta \approx 0$, and the interference is well cancelled. Note that this definition is arbitrary and constitutes an example based on the processing of [45]. The framework can be used with any other function of residuals which depends on S_R and S_C only.
3) A perfect IC is performed at both functions simultaneously, leading to null residuals:
$$\zeta_R = 0 \quad \text{and} \quad \zeta_C = 0. \tag{57}$$

Note that the metric proposed in [44] is equivalent to the particular case where perfect IC is performed at one function and no IC is performed at the other function. Proposition 7 extends the results of Section III to integrate IC in the metrics.

Proposition 7: *To integrate IC in the metrics of Section III, Propositions 1 to 6 are extended by modifying the functions*

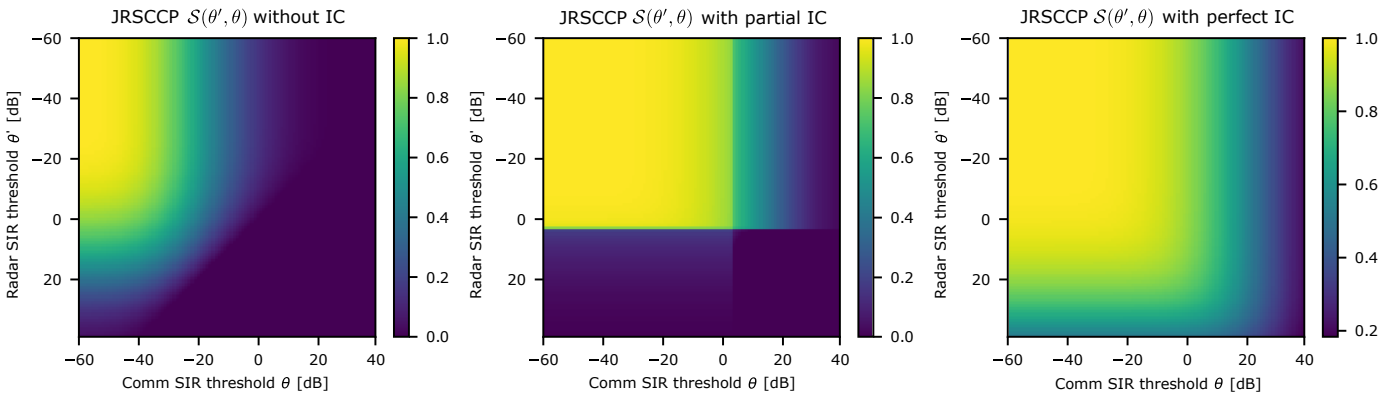


Fig. 11. JRSCCP metric with different IC schemes.

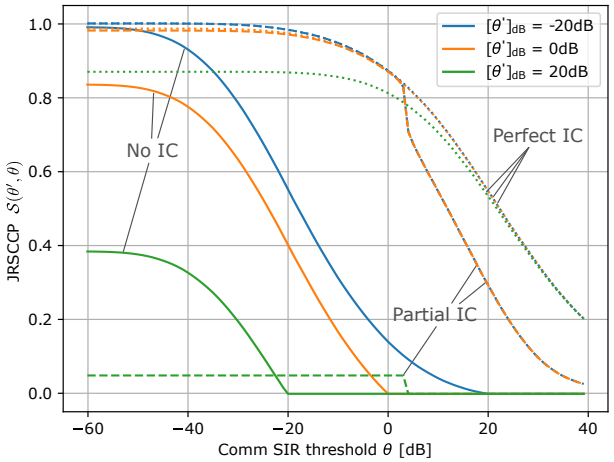


Fig. 12. JRSCCP metric with different IC schemes, for fixed radar SIR thresholds $\theta' = \{-20, 0, 20\}$dB.

and regions of integration following the expressions given in the third column of Table I.

Proof: The proof is detailed in Appendices A and B. ■

The upper and lower bounds in Corollary 1 are also generalised for the joint metrics with IC using the different metrics of Table I and the Fréchet inequalities. The same applies with the Bayes law for the conditional metrics, rewritten as follows:

$$\mathcal{P}^{\text{IC}}_{\text{C|D}}(\theta;\gamma) = \mathbb{P}\left(\frac{S_C}{\zeta_R+I} \geq \theta \,\middle|\, S_R\kappa+\zeta_C+I \geq \gamma\right) \quad (58)$$

for a given $\mathcal{P}^{\text{IC}}_{\text{FA}}(\gamma)$,

$$\mathcal{P}^{\text{IC}}_{\text{C|S}}(\theta;\theta') = \mathbb{P}\left(\frac{S_C}{\zeta_R+I} \geq \theta \,\middle|\, \frac{S_R\kappa}{\zeta_C+I} \geq \theta'\right). \quad (59)$$

$$\mathcal{P}^{\text{IC}}_{\text{D|C}}(\gamma;\theta) = \mathbb{P}\left(S_R\kappa+\zeta_C+I \geq \gamma \,\middle|\, \frac{S_C}{\zeta_R+I} \geq \theta\right) \quad (60)$$

for a given $\mathcal{P}^{\text{IC}}_{\text{FA}}(\gamma)$,

$$\mathcal{P}^{\text{IC}}_{\text{S|C}}(\theta';\theta) = \mathbb{P}\left(\frac{S_R\kappa}{\zeta_C+I} \geq \theta' \,\middle|\, \frac{S_C}{\zeta_R+I} \geq \theta\right). \quad (61)$$

Figure 11 and 12 illustrate the impact of the different IC schemes on the JRSCCP metric: no IC, partial IC with $a = 0.5$ and $b = 2$, or perfect IC. This choice of parameters is obtained after fitting the residuals obtained with the processing of [45]. With partial IC, the achieved performance depends on the considered radar and communication SIR thresholds. At high radar (resp. communication) SIR thresholds, it is likely that the radar (resp. communication) signal is dominant for the metric to be non zero. In that situation, the IC performs well at the communication (resp. radar) function, but the interference level may increase at the other function. Therefore, depending on the considered pair of thresholds, the performance is either improved or worsened by the IC scheme. For instance, for high radar SIR thresholds, the achieved performance are drastically worsened with partial IC, as the residual interference at the communication function is increasing with the radar echo power owing to the poor communication parameters' estimation. With perfect IC, the performance drastically increases since the interference power is in most cases lower than the radar and communication powers. In both cases, when partial or perfect IC is introduced, condition (28) does not apply anymore. The coupling of both functions becomes limited. It therefore enables to reach higher radar and communication requirements to some extent.

B. Multi-lane Scenario

Following the system model of [24], the two-lane automotive scenario can be generalised to an M-lane scenario, by adapting the preliminary results of Figure 3, i.e. the PDFs of S_R and S_C and the LT of I. Let us now denote by d the width of one lane, and d_L the perpendicular distance between the RSUs and the center of the nearest lane, as illustrated in Figure 13. In the two-lane scenario, $d_I = d$ and $d_C = d_L$. Let us now assume that the typical vehicle is located in the m^{th} lane starting from the center of the road.

a) Communication signal: The perpendicular distance to the communication signal becomes $d_C = (M-m)d+d_L$. The minimum distance $r_{C\text{min}}$ and the PDF of S_C are then updated by plugging the new distance d_C.

b) Interfering signal: The perpendicular distance to the n^{th} interfering lane (starting from the center of the road), is $d_{I,n} = (m+n-1)d$. The minimum distance $r_{I\text{min},n}$ to the n^{th} interfering lane is then obtained by plugging the new distance

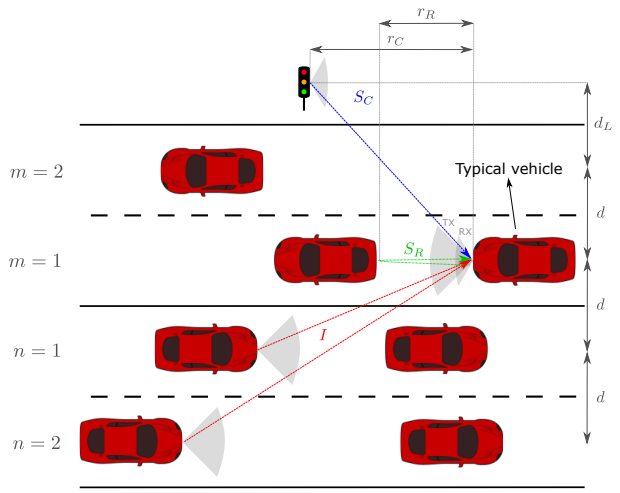


Fig. 13. Multi-lane road scenario with $M = 2$.

$d_{I,n}$. The total interference at the typical user is finally given by

$$I = \sum_{n=1}^{M} \sum_{i \mid x_i \in \mathbf{\Phi}_{I,n}} \rho_I \left(x_i^2 + d_{I,n}^2\right)^{-\frac{\alpha_I}{2}} |h_{n,i}|^2, \qquad (62)$$

where $\mathbf{\Phi}_{I,n}$ are independent PPPs modelling the interfering nodes on each lane, and $h_{n,i}$ are the independent small-scale fadings associated to each interfering link. Based on that, the LT of I is updated as

$$\mathcal{L}_I(s) = \exp\left(-\lambda_I \sum_{n=1}^{M} \int_{r_{I\min,n}}^{\infty} \left(1 - \mathcal{L}_{|h_{i,n}|^2}\left(s\chi_n(r)\right)\right) \mathrm{d}r\right), \qquad (63)$$

where $\chi_n(r) = \rho_I \left(r^2 + d_{I,n}^2\right)^{-\frac{\alpha_I}{2}}$ owing to the independence of the different interfering PPPs and small-scale fadings.

Further improvements could include numerous other sources of interference considered in [27], [46], and the blockage induced by the vehicles as studied in [47].

VI. Possible Generalisations

A. Other Point Processes

PPPs enable to efficiently model random node locations owing to their tractability and analytical flexibility. Other existing Point Processes (PP) are by contrast more accurate for modelling real world scenarios at the price of a higher complexity [19]. In order to generalise the framework to integrate such PPs, the preliminary results of Figure 3 (the PDFs of S_R and S_C and the LT of I) should be adapted to the considered PP. Owing to the high mathematical complexity induced by such PPs, these functions can be approximated if needed. For instance, [48] approximates the LT of the interference using a sigmoidal approximation, or following a transformed distribution approach. Another interesting proposal is presented in [49] to approximate any PP as two inhomogeneous PPPs through inhomogeneous double thinning. In that case, an equivalent network model is introduced based on two independent inhomogeneous PPPs in order approximate the original PP and obtain tractable results. The introduction of inhomogeneous PPPs in all the results of this paper is then straightforward with the considered system model.

B. Non-automotive Scenarios

The presented metrics can be applied to any full-duplex joint radar-communication scenario in which a joint radar-communication system simultaneously receives a radar and an uplink communication signal while suffering from interference, as illustrated in Figure 1. Two examples of such scenarios are here described.

a) Indoor scenario (e.g. [50], [51]): an Access Point (AP) equipped with a DFRC system is detecting User Equipments (UE), while receiving simultaneously a communication signal from the same or another UE. The AP is suffering from interference coming from other APs and/or other UEs.

b) Crowd sensing (e.g. [52]): a Base Station (BS) equipped with a DFRC system is serving and tracking multiple UEs. The BS is simultaneously receiving data from another macro-BS or from the UEs while tracking them. The BS is suffering from interference coming from other BSs and/or other UEs.

In any case, the system models should be modified accordingly to the scenario. For instance, both scenarios are now two-dimensional. The new system models are not further developed in this manuscript owing to space limitation.

VII. Conclusion

In this paper, a new automotive scenario with RSUs and vehicles, both equipped with DFRC systems, has been analysed. In order to analyse the performance of both functions separately and jointly, multiple metrics have been developed using stochastic geometry. Based on that, optimisation of the transmit powers and density of the RSUs and vehicles has also been performed. Finally, the metrics have been extended to include a new model of IC at both functions. Other extensions and generalisations have been discussed.

In future works, other models and schemes for the IC could be considered, i.e. suppressing the interference at the radar or communication function only. Additionally, the proposed generalisations should be deeper analysed. Finally, the developed metrics can be evaluated using other tools and frameworks (e.g. ray-tracing simulations).

References

[1] L. Zheng, M. Lops, Y. C. Eldar, and X. Wang, "Radar and communication coexistence: an overview: a review of recent methods," *IEEE Signal Process. Mag.*, vol. 36, no. 5, pp. 85–99, 2019.

[2] N. C. Luong, X. Lu, D. T. Hoang, D. Niyato, and D. I. Kim, "Radio resource management in joint radar and communication: a comprehensive survey," *IEEE Commun. Surv. Tutor.*, vol. 23, no. 2, pp. 780–814, 2021.

[3] F. Liu and C. Masouros, "A tutorial on joint radar and communication transmission for vehicular networks—Part I: background and fundamentals," *IEEE Commun. Lett.*, vol. 25, no. 2, pp. 322–326, 2021.

[4] S. Singh, X. Zhang, and J. G. Andrews, "Joint rate and SINR coverage analysis for decoupled uplink-downlink biased cell associations in hetnets," *IEEE Trans. Wirel. Commun.*, vol. 14, no. 10, pp. 5360–5373, 2015.

[5] M. Di Renzo and W. Lu, "System-level analysis and optimization of cellular networks with simultaneous wireless information and power transfer: stochastic geometry modeling," *IEEE Trans. Veh. Technol.*, vol. 66, no. 3, pp. 2251–2275, 2017.

[6] A. Munari, L. Simić, and M. Petrova, "Stochastic geometry interference analysis of radar network performance," *IEEE Commun. Lett.*, vol. 22, no. 11, pp. 2362–2365, 2018.
[7] S. S. Ram, G. Singh, and G. Ghatak, "Estimating radar detection coverage probability of targets in a cluttered environment using stochastic geometry," in *RADARConf20*, 2020, pp. 665–670.
[8] ——, "Optimization of radar parameters for maximum detection probability under generalized discrete clutter conditions using stochastic geometry," *IEEE Open J. Signal Process.*, vol. 2, pp. 571–585, 2021.
[9] S. S. Ram and G. Ghatak, "Estimation of bistatic radar detection performance under discrete clutter conditions using stochastic geometry," in *RadarConf22*, 2022, pp. 1–6.
[10] J. Park and R. W. Heath, "Analysis of blockage sensing by radars in random cellular networks," *IEEE Signal Process. Lett.*, vol. 25, no. 11, pp. 1620–1624, 2018.
[11] P. Ren, A. Munari, and M. Petrova, "Performance tradeoffs of joint radar-communication networks," *IEEE Wirel. Commun. Lett.*, vol. 8, no. 1, pp. 165–168, 2019.
[12] ——, "Performance analysis of a time-sharing joint radar-communications network," in *ICNC 2020*, 2020, pp. 908–913.
[13] M. Kafafy, A. S. Ibrahim, and M. H. Ismail, "Stochastic geometry-based performance analysis of cellular systems in the vicinity of rotating radars," *IEEE Commun. Lett.*, vol. 25, no. 4, pp. 1391–1395, 2021.
[14] R. M. Rao, H. S. Dhillon, V. Marojevic, and J. H. Reed, "Underlay radar-massive MIMO spectrum sharing: modeling fundamentals and performance analysis," *IEEE Trans. Wirel. Commun.*, vol. 20, no. 11, pp. 7213–7229, 2021.
[15] C. Skouroumounis, C. Psomas, and I. Krikidis, "Cooperative detection for mmWave radar-communication systems," in *ICC workshops 2020*, 2020, pp. 1–6.
[16] ——, "FD-JCAS techniques for mmWave hetnets: Ginibre point process modeling and analysis," *IEEE Trans. Mob. Comput.*, vol. 21, no. 12, pp. 4352–4366, 2022.
[17] Z. Fang, Z. Wei, Z. Feng, X. Chen, and Z. Guo, "Performance of joint radar and communication enabled cooperative detection," in *ICCC 2019*, 2019, pp. 753–758.
[18] S. S. Ram and G. Ghatak, "Optimization of network throughput of joint radar communication system using stochastic geometry," pp. 1–23, 2022. [Online]. Available: http://arxiv.org/abs/2201.03221
[19] Y. Hmamouche, M. Benjillali, S. Saoudi, H. Yanikomeroglu, and M. D. Renzo, "New trends in stochastic geometry for wireless networks: a tutorial and survey," *Proc. IEEE*, vol. 109, no. 7, pp. 1200–1252, 2021.
[20] F. Baccelli and B. Blaszczyszyn, *Stochastic Geometry and Wireless Networks: Volume I Theory*, 2010.
[21] ——, *Stochastic Geometry and Wireless Networks: Volume II Applications*, 2010.
[22] H. ElSawy, E. Hossain, and M. Haenggi, "Stochastic geometry for modeling, analysis, and design of multi-tier and cognitive cellular wireless networks: a survey," *IEEE Commun. Surv. Tutor.*, vol. 15, no. 3, pp. 996–1019, 2013.
[23] M. Haenggi, J. G. Andrews, F. Baccelli, O. Dousse, and M. Franceschetti, "Stochastic geometry and random graphs for the analysis and design of wireless networks," *IEEE IEEE J. Sel. Areas Commun.*, vol. 27, no. 7, pp. 1029–1046, 2009.
[24] Z. Fang, Z. Wei, X. Chen, H. Wu, and Z. Feng, "Stochastic geometry for automotive radar interference with RCS characteristics," *IEEE Wirel. Commun. Lett.*, vol. 9, no. 11, pp. 1817–1820, 2020.
[25] A. Al-Hourani, R. J. Evans, S. Kandeepan, B. Moran, and H. Eltom, "Stochastic geometry methods for modeling automotive radar interference," *IEEE Trans. Intell. Transp. Syst.*, vol. 19, no. 2, pp. 333–344, 2018.
[26] K. V. Mishra, B. Shankar M.R., and B. Ottersten, "Stochastic-geometry-based interference modeling in automotive radars using Matérn hard-core process," in *RadarConf20*, 2020, pp. 1–5.
[27] Z. Fang, Z. Wei, H. Ma, X. Chen, and Z. Feng, "Analysis of automotive radar interference among multiple vehicles," in *WCNCW 2020*, 2020, pp. 1–6.
[28] P. Chu, J. A. Zhang, X. Wang, Z. Fei, G. Fang, and D. Wang, "Interference characterization and power optimization for automotive radar with directional antenna," *IEEE Trans. Veh. Technol.*, vol. 69, no. 4, pp. 3703–3716, 2020.
[29] G. Ghatak, S. S. Kalamkar, Y. Gupta, and S. Sharma, "A fine-grained analysis of radar detection in vehicular networks," in *GLOBECOM 2021*, 2021, pp. 01–06.
[30] G. Ghatak, S. Kalamkar, and Y. Gupta, "Radar detection in vehicular networks: fine-grained analysis and optimal channel access," *IEEE Trans. Veh. Technol.*, pp. 1–1, 2022.
[31] H. Ma, Z. Wei, X. Chen, Z. Fang, Y. Liu, F. Ning, and Z. Feng, "Performance analysis of joint radar and communication enabled vehicular ad hoc network," in *ICCC 2019*, 2019, pp. 887–892.
[32] D. Ghozlani, A. Omri, S. Bouallegue, H. Chamkhia, and R. Bouallegue, "Stochastic geometry-based analysis of joint radar and communication-enabled cooperative detection systems," in *WiMob 2021*, 2021, pp. 325–330.
[33] J. Marcum, "A statistical theory of target detection by pulsed radar," *IRE Trans. Inf. Theory*, vol. 6, no. 2, pp. 59–267, 1960.
[34] J. Gil-Pelaez, "Note on the inversion theorem," *Biometrika*, vol. 38, no. 3-4, pp. 481–482, 12 1951. [Online]. Available: https://doi.org/10.1093/biomet/38.3-4.481
[35] H. Friis, "A note on a simple transmission formula," *Proc. IRE*, vol. 34, no. 5, pp. 254–256, 1946.
[36] M. A. Richards, *Fundamentals of Radar Signal Processing*. McGraw-Hill Professional, 2005.
[37] P. Swerling, "Probability of detection for fluctuating targets," *IRE Trans. Inf. Theory*, vol. 6, no. 2, pp. 269–308, 1960.
[38] S. Wang, W. Guo, and M. D. McDonnell, "Distance distributions for real cellular networks," in *INFOCOM 2014 WKSHPS*, 2014, pp. 181–182.
[39] H. ElSawy, A. Sultan-Salem, M.-S. Alouini, and M. Z. Win, "Modeling and analysis of cellular networks using stochastic geometry: a tutorial," *IEEE Commun. Surv. Tutor.*, vol. 19, no. 1, pp. 167–203, 2017.
[40] F. D. S. Moulin, C. Wiame, C. Oestges, and L. Vandendorpe, "Stochastic geometry-based modelling of mobile uav relay networks under realistic fading," in *VTC2021-Spring*, 2021, pp. 1–7.
[41] A. R. Chiriyath, B. Paul, and D. W. Bliss, "Radar-communications convergence: coexistence, cooperation, and co-design," *IEEE Trans. Cogn. Commun. Netw.*, vol. 3, no. 1, pp. 1–12, 2017.
[42] M. Fréchet, "Généralisation du théorème des probabilités totales," *Fundamenta Mathematicae*, vol. 25, no. 1, pp. 379–387, 1935. [Online]. Available: http://eudml.org/doc/212798
[43] Z. Tong and M. Haenggi, "Throughput analysis for full-duplex wireless networks with imperfect self-interference cancellation," *IEEE Trans. Commun.*, vol. 63, no. 11, pp. 4490–4500, 2015.
[44] J. Blomer and N. Jindal, "Transmission capacity of wireless ad hoc networks: successive interference cancellation vs. joint detection," in *IEEE ICC*, 2009, pp. 1–5.
[45] F. De Saint Moulin, C. Oestges, and L. Vandendorpe, "Characterisation and cancellation of interference with multiple phase-coded fmcw dual-function radar communication systems," in *2022 IEEE 95th Vehicular Technology Conference: (VTC2022-Spring)*, 2022, pp. 1–7.
[46] L. Kui, S. Huang, and Z. Feng, "Interference analysis for automotive radar using matérn hard-core point process," in *2021 IEEE/CIC ICCC*, 2021, pp. 817–822.
[47] C.-S. Choi and F. Baccelli, "A stochastic geometry model for spatially correlated blockage in vehicular networks," *IEEE Internet Things J.*, vol. 9, no. 20, pp. 19 881–19 889, 2022.
[48] F. J. Martin-Vega, G. Gomez, M. C. Aguayo-Torres, and M. Di Renzo, "Analytical modeling of interference aware power control for the uplink of heterogeneous cellular networks," *IEEE Trans. Wirel. Commun*, vol. 15, no. 10, pp. 6742–6757, 2016.
[49] M. Di Renzo, S. Wang, and X. Xi, "Inhomogeneous double thinning—modeling and analysis of cellular networks by using inhomogeneous poisson point processes," *IEEE Trans. Wirel. Commun.*, vol. 17, no. 8, pp. 5162–5182, 2018.
[50] C. Jiao, Z. Zhang, C. Zhong, and Z. Feng, "An indoor mmwave joint radar and communication system with active channel perception," in *IEEE ICC*, 2018, pp. 1–6.
[51] L. Storrer, H. C. Yildirim, M. Crauwels, E. I. P. Copa, S. Pollin, J. Louveaux, P. De Doncker, and F. Horlin, "Indoor tracking of multiple individuals with an 802.11ax wi-fi-based multi-antenna passive radar," *IEEE Sens. J.*, vol. 21, no. 18, pp. 20 462–20 474, 2021.
[52] L. Storrer, H. C. Yildirim, M. Willame, J. Louveaux, P. De Doncker, S. Pollin, and F. Horlin, "Crowd counting model training with the method of moments in electromagnetics," in *IEEE 3rd Int. Symp. on Joint Comm. & Sens. (JC&S)*, 2023, pp. 1–6.

APPENDIX A
JRSCCP AND DERIVED METRICS

In this appendix, the JRSCCP metric with and without IC are first developed. Then, the coverage and success probabilities are obtained from the expressions of the JRSCCP metric.

A. JRSCCP metric

1) With IC: The JRSCCP metric with IC can be developed as

$$\mathcal{S}(\theta',\theta) = \mathbb{P}_{S_R,S_C,I}\left(\frac{S_R\kappa}{S_C+I} \geq \theta', \frac{S_C}{S_R+I} \geq \theta\right)$$
$$= \mathbb{E}_{S_R,S_C}\left[\mathbb{P}_{I|S_R,S_C}\left(I \leq \frac{S_R\kappa}{\theta'} - \zeta_C, I \leq \frac{S_C}{\theta} - \zeta_R\right)\right].$$

This probability is non zero either if

$$\begin{cases} \frac{S_R\kappa}{\theta'} - \zeta_C \geq 0 \\ \frac{S_C}{\theta} - \zeta_R \geq \frac{S_R\kappa}{\theta'} - \zeta_C \end{cases}, \text{ or } \begin{cases} \frac{S_C}{\theta} - \zeta_R \geq 0 \\ \frac{S_R\kappa}{\theta'} - \zeta_C \geq \frac{S_C}{\theta} - \zeta_R \end{cases}, \tag{64}$$

leading to the areas $\Omega_{\text{S1}}^{\text{IC}}$ and $\Omega_{\text{S2}}^{\text{IC}}$ given in Table I, including the radar and communication power constraints. In $\Omega_{\text{S1}}^{\text{IC}}$, applying the Gil-Pelaez theorem,

$$\mathbb{P}_{I|S_R,S_C}\left(I \leq \frac{S_R\kappa}{\theta'} - \zeta_C, I \leq \frac{S_C}{\theta} - \zeta_R\right)$$
$$= \mathbb{P}_{I|S_R,S_C}\left(I \leq \frac{S_R\kappa}{\theta'} - \zeta_C\right)$$
$$= \frac{1}{2} - \frac{1}{\pi}\int_0^\infty \frac{1}{\tau}\,\text{Im}\left\{\mathcal{L}_I(-j\tau)\,\psi_{\text{S1}}^{\text{IC}}(-j\tau)\right\}\text{d}\tau,$$

with $\psi_{\text{S1}}^{\text{IC}}$ given in Table I. In $\Omega_{\text{S2}}^{\text{IC}}$, applying the Gil-Pelaez theorem,

$$\mathbb{P}_{I|S_R,S_C}\left(I \leq \frac{S_R\kappa}{\theta'} - \zeta_C, I \leq \frac{S_C}{\theta} - \zeta_R\right)$$
$$= \mathbb{P}_{I|S_R,S_C}\left(I \leq \frac{S_C}{\theta} - \zeta_R\right)$$
$$= \frac{1}{2} - \frac{1}{\pi}\int_0^\infty \frac{1}{\tau}\,\text{Im}\left\{\mathcal{L}_I(-j\tau)\,\psi_{\text{S2}}^{\text{IC}}(-j\tau)\right\}\text{d}\tau,$$

with $\psi_{\text{S2}}^{\text{IC}}$ given in Table I.

2) Without IC: Without IC, the JRSCCP is non zero only if

$$\begin{cases} \frac{S_R\kappa}{\theta'} - S_C \geq 0 \\ \frac{S_C}{\theta} - S_R \geq 0 \end{cases} \quad \Leftrightarrow \quad \theta S_R \leq S_C \leq \frac{S_R\kappa}{\theta'},$$

which is fulfilled only if

$$\theta\theta' \leq \kappa \quad \Leftrightarrow \quad [\theta]_{\text{dB}} + [\theta']_{\text{dB}} \leq [\kappa]_{\text{dB}}.$$

Then, conditions of (64) are respectively rewritten as

$$\begin{cases} S_R\frac{\theta(\theta'+\kappa)}{\theta'(\theta+1)} \leq S_C \leq \frac{S_R\kappa}{\theta'} \\ \theta S_R \leq S_C \leq S_R\frac{\theta(\theta'+\kappa)}{\theta'(\theta+1)} \end{cases},$$

leading to the areas Ω_{S1} and Ω_{S2} given in Table I, including the radar and communication power constraints. Finally, the functions $\psi_{\text{S1}}^{\text{IC}}$ and $\psi_{\text{S2}}^{\text{IC}}$ are rewritten as ψ_{S1} and ψ_{S2} of Table I, leading to (29).

B. Coverage probability

1) With IC: The coverage probability is obtained as $\mathcal{P}_{\text{C}}^{\text{IC}}(\theta) = \lim_{\theta'\to 0}\mathcal{S}^{\text{IC}}(\theta',\theta)$. In that case, $\Omega_{\text{S1}}^{\text{IC}}$ vanishes and $\Omega_{\text{S2}}^{\text{IC}}$ becomes Ξ_C^{IC} of Table I.

2) Without IC: Without IC, $\psi_{\text{S2}}^{\text{IC}}$ and Ξ_C^{IC} are respectively rewritten as ξ_C and Ξ_C given in Table I.

C. Success probability

1) With IC: The success probability is obtained as $\mathcal{P}_{\text{S}}^{\text{IC}}(\theta') = \lim_{\theta\to 0}\mathcal{S}^{\text{IC}}(\theta',\theta)$. In that case, $\Omega_{\text{S2}}^{\text{IC}}$ vanishes and $\Omega_{\text{S1}}^{\text{IC}}$ becomes Ξ_C^{IC} of Table I.

2) Without IC: Without IC, $\psi_{\text{S1}}^{\text{IC}}$ and Ξ_S^{IC} are respectively rewritten as ξ_S and Ξ_S given in Table I.

APPENDIX B
JRDCCP AND DERIVED METRICS

In this appendix, the JRDCCP metric with and without IC are first developed. Then, the detection and false alarm probabilities are obtained from the expressions of the JRDCCP metric.

A. JRDCCP metric

1) With IC: The JRDCCP metric can be developed as

$$\mathcal{D}^{\text{IC}}(\theta;\gamma) = \mathbb{P}_{S_R,S_C,I}\left(S_R\kappa + \zeta_C + I \geq \gamma, \frac{S_C}{\zeta_R+I} \geq \theta\right)$$
$$= \mathbb{E}_{S_R,S_C}\left[\mathbb{P}_{I|S_R,S_C}\left(\gamma - S_R\kappa - \zeta_C \leq I \leq \frac{S_C}{\theta} - \zeta_R\right)\right].$$

This probability is non zero either when

$$\begin{cases} \gamma - S_R\kappa - \zeta_C \leq 0 \\ \frac{S_C}{\theta} - \zeta_R \geq 0 \end{cases}, \text{ or } \begin{cases} \gamma - S_R\kappa - \zeta_C \geq 0 \\ \frac{S_C}{\theta} - \zeta_R \geq \gamma - S_R\kappa - \zeta_C \end{cases}, \tag{65}$$

leading to the areas $\Omega_{\text{D1}}^{\text{IC}}$ and $\Omega_{\text{D2}}^{\text{IC}}$ given in Table I, including the radar and communication power constraints. In $\Omega_{\text{D1}}^{\text{IC}}$, applying the Gil-Pelaez theorem,

$$\mathbb{P}_{I|S_R,S_C}\left(I \leq \frac{S_C}{\theta} - \zeta_R\right) =$$
$$\frac{1}{2} - \frac{1}{\pi}\int_0^\infty \frac{1}{\tau}\,\text{Im}\left\{\mathcal{L}_I(-j\tau)\,\psi_{\text{D1}}^{\text{IC}}(-j\tau)\right\}\text{d}\tau,$$

with $\psi_{\text{D1}}^{\text{IC}}$ given in Table I. In $\Omega_{\text{D2}}^{\text{IC}}$, applying the Gil-Pelaez theorem,

$$\mathbb{P}_{I|S_R,S_C}\left(\gamma - S_R\kappa - \zeta_C \leq I \leq \frac{S_C}{\theta} - \zeta_R\right)$$
$$= \mathbb{P}_{I|S_R,S_C}\left(I \leq \frac{S_C}{\theta} - \zeta_R\right)$$
$$- \mathbb{P}_{I|S_R,S_C}\left(I \leq \gamma - S_R\kappa - \zeta_C\right)$$
$$= -\frac{1}{\pi}\int_0^\infty \frac{1}{\tau}\,\text{Im}\left\{\mathcal{L}_I(-j\tau)\,\psi_{\text{D2}}^{\text{IC}}(-j\tau)\right\}\text{d}\tau,$$

with $\psi_{\text{D2}}^{\text{IC}}$ given in Table I.

2) Without IC: Without IC, conditions of (65) are respectively rewritten as

$$\begin{cases} S_C \geq \max\left(\theta S_R, \gamma - S_R\kappa\right) \\ \dfrac{\theta\gamma}{\theta+1} - S_R\dfrac{\theta(\kappa-1)}{\theta+1} \leq S_C \leq \gamma - \kappa S_R \end{cases},$$

leading to the areas Ω_{D1} and Ω_{D2} given in Table I, including the radar and communication power constraints. Finally, the functions $\psi_{\mathrm{D1}}^{\mathrm{IC}}$ and $\psi_{\mathrm{D2}}^{\mathrm{IC}}$ are replaced by ψ_{D1} and ψ_{D2} of Table I, leading to (26).

B. Detection probability

1) With IC: The detection probability is obtained as $\mathcal{P}_{\mathrm{D}}^{\mathrm{IC}}(\gamma) = \lim_{\theta\to 0}\mathcal{D}^{\mathrm{IC}}(\theta;\gamma)$. In that case, the area $\Omega_{\mathrm{D2}}^{\mathrm{IC}}$ and $\Omega_{\mathrm{D1}}^{\mathrm{IC}}$ are restricted to Ξ_D^{IC} and $\Xi_D^{\mathrm{IC}^c}$ of Table I, where $\cdot^c$ denotes the complement set. In $\Xi_D^{\mathrm{IC}^c}$, we have

$$\lim_{\theta\to 0}\mathbb{P}_{I|S_R,S_C}\left(I \leq \frac{S_C}{\theta} - \zeta_R\right) = 1.$$

In Ξ_D^{IC}, we have

$$\begin{aligned} &\lim_{\theta\to 0}\mathbb{P}_{I|S_R,S_C}\left(\gamma - S_R\kappa - \zeta_C \leq I \leq \frac{S_C}{\theta} - \zeta_R\right) \\ &= \mathbb{P}_{I|S_R,S_C}\left(I \geq \gamma - S_R\kappa - \zeta_C\right) \\ &= \frac{1}{2} + \frac{1}{\pi}\int_0^\infty \frac{1}{\tau}\,\mathrm{Im}\left\{\mathcal{L}_I(-j\tau)\,\xi_D^{\mathrm{IC}}(-j\tau)\right\}\mathrm{d}\tau, \end{aligned}$$

with ξ_D^{IC} given in Table I. Finally, the final result is obtained knowing that

$$\mathcal{E}_{\Xi_D^{\mathrm{IC}^c}}[1] = 1 - \mathcal{E}_{\Xi_D^{\mathrm{IC}}}[1].$$

2) Without IC: Without IC, ξ_D^{IC} and Ξ_D^{IC} are respectively rewritten as ξ_D and Ξ_D of Table I.

C. False alarm probability

1) With IC: The false alarm probability with IC is identical to the detection probability with IC, except that the radar echo is suppressed from the received power. In that case, ξ_D^{IC} and Ξ_D^{IC} are replaced by ξ_F^{IC} and Ξ_F^{IC} given in Table I.

2) Without IC: Without IC, ξ_D^{IC} and Ξ_F^{IC} are respectively rewritten as ξ_F and Ξ_F of Table I.



François De Saint Moulin received the B.Sc. and the M.Sc. degrees in 2018 and 2020, respectively, in electrical engineering from the Université catholique de Louvain, (UCLouvain), Louvain-la-Neuve, Belgium, where he is currently working toward the Ph.D. degree with the Institute for Information and Communication Technologies, Electronics and Applied Mathematics, (ICTEAM), UCLouvain. His research interests include integrated sensing and communication technologies, and stochastic geometry.



Charles Wiame (Student member, IEEE) obtained the M.Sc. degree in electrical engineering from UCLouvain, Belgium, in 2017. He is currently teaching assistant and Ph.D student at UCLouvain, working under the supervision of Prof. L. Vandendorpe and Prof. C. Oestges. In 2022, he was a visitor at the Kungliga Tekniska högskolan, Stockholm, Sweden. His current research interests include the joint analysis of coverage and EMF exposure in wireless networks, user-centric cell-free systems and stochastic geometry.



Luc Vandendorpe (Fellow, IEEE) was born in Mouscron, Belgium, in 1962. He received the degree (summa cum laude) in electrical engineering and the Ph.D. degree in applied science from UCLouvain, Louvain-la-Neuve, Belgium, in 1985 and 1991, respectively. Since 1985, he has been with the Communications and Remote Sensing Laboratory, UCL, where he first worked in the field of bit rate reduction techniques for video coding. In 1992, he was a Visiting Scientist and a Research Fellow with the Telecommunications and Traffic Control Systems Group, Delft Technical University, The Netherlands, where he worked on spread spectrum techniques for personal communications systems. From October 1992 to August 1997, he was a Senior Research Associate with the Belgian NSF, UCL, and an invited Assistant Professor. He is currently a Full Professor with the Institute for Information and Communication Technologies, Electronics and Applied Mathematics, UCLouvain. His research interests include digital communication systems and more precisely resource allocation for OFDM(A)-based multicell systems, MIMO and distributed MIMO, sensor networks, UWB-based positioning, and wireless power transfer. He is or has been a TPC Member for numerous IEEE conferences, such as VTC, GLOBECOM, SPAWC, ICC, PIMRC, and WCNC. He was an Elected Member of the Signal Processing for Communications Committee from 2000 to 2005 and the Sensor Array and Multichannel Signal Processing Committee of the Signal Processing Society from 2006 to 2008 and from 2009 to 2011. He was the Chair of the IEEE Benelux Joint Chapter on communications and vehicular technology from 1999 to 2003. He was the Co-Technical Chair of IEEE ICASSP 2006. He served as an Editor of synchronization and equalization for IEEE TRANSACTIONS ON COMMUNICATIONS from 2000 to 2002 and as an Associate Editor for IEEE TRANSACTIONS ON WIRELESS COMMUNICATIONS from 2003 to 2005 and IEEE TRANSACTIONS ON SIGNAL PROCESSING from 2004 to 2006.



Claude Oestges received the M.Sc. and Ph.D. degrees in Electrical Engineering from UCLouvain, Louvain-la-Neuve, Belgium, respectively in 1996 and 2000. In January 2001, he joined as a post-doctoral scholar the Smart Antennas Research Group (Information Systems Laboratory), Stanford University, CA, USA. From January 2002 to September 2005, he was associated with the Microwave Laboratory UCLouvain as a post-doctoral fellow of the Belgian Fonds de la Recherche Scientifique (FRS-FNRS). Claude Oestges is presently Full Professor with the Electrical Engineering Department, Institute for Information and Communication Technologies, Electronics and Applied Mathematics (ICTEAM), UCLouvain. He is the author or co-author of four books and more than 200 journal papers and conference communications, and he was the chair of COST Action CA15104 IRACON (2016-2020), as well as the recipient of the 1999-2000 IET Marconi Premium Award and of the IEEE Vehicular Technology Society Neal Shepherd Award in 2004 and 2012.